TITLE

Diagnostic Utility of Genome-wide DNA Methylation Analysis in Genetically Unsolved Developmental and Epileptic Encephalopathies and Refinement of a CHD2 Episignature

AUTHORS AND AFFILIATIONS

Christy W. LaFlamme[1,2*], Cassandra Rastin[3,4*], Soham Sengupta[1], Helen E. Pennington[1,5], Sophie J. Russ-Hall[6], Amy L. Schneider[6], Emily S. Bonkowski[1], Edith P. Almanza Fuerte[1], Miranda Galey[7], Joy Goffena[7], Sophia B. Gibson[7,8], Talia J. Allan[6], Denis M. Nyaga[9], Nico Lieffering[9], Malavika Hebbar[7], Emily V. Walker[10], Daniel Darnell[10], Scott R. Olsen[10], Pandurang Kolekar[11], Nahdir Djekidel[12], Wojciech Rosikiewicz[12], Haley McConkey[4], Jennifer Kerkhof[4], Michael A. Levy[4], Raissa Relator[4], Dorit Lev[13], Tally Lerman-Sagie[14,15], Kristen L. Park[16], Marielle Alders[17], Gerarda Cappuccio[18,19], Nicolas Chatron[20,21], Leigh Demain[22], David Genevieve[23], Gaetan Lesca[20,21], Tony Roscioli[24-27], Damien Sanlaville[20,21], Matthew L. Tedder[28], Monika Weisz Hubshman[29,30], Shamika Ketkar[29], Hongzheng Dai[29], Kim Carlyle Worley[29], Jill A. Rosenfeld[29], Hsiao-Tuan Chao[29,31-35], Undiagnosed Diseases Network, Geoffrey Neale[10], Gemma L. Carvill[36], University of Washington Center for Rare Disease Research, Zhaoming Wang[11,37], Samuel F. Berkovic[6], Lynette G. Sadleir[9], Danny E. Miller[7,38-39], Ingrid E. Scheffer[6,40-41], Bekim Sadikovic[3,4#], Heather C. Mefford[1#]

[1]Center for Pediatric Neurological Disease Research, St. Jude Children's Research Hospital, Memphis, TN 38105, USA

[2]Graduate School of Biomedical Sciences, St. Jude Children's Research Hospital, Memphis, TN 38105, USA

[3]Department of Pathology & Laboratory Medicine, Western University, London, Ontario, N5A 3K7, Canada

[4]Verspeeten Clinical Genome Centre, London Health Science Centre, London, Ontario, N6A 5W9, Canada

[5]Department of Mathematics & Statistics, Rhodes College, Memphis, TN 38112, USA

[6]Epilepsy Research Centre, Department of Medicine, University of Melbourne, Austin Health, Heidelberg, Victoria 3084, Australia

[7]Division of Genetic Medicine, Department of Pediatrics, University of Washington and Seattle Children's Hospital, Seattle, WA 98195, USA

[8]Department of Genome Sciences, University of Washington School of Medicine, Seattle, WA 98195, USA

[9]Department of Paediatrics and Child Health, University of Otago, Wellington 6242, New Zealand

[10]Hartwell Center for Bioinformatics and Biotechnology, St. Jude Children's Research Hospital Memphis, TN 38105, USA

[11]Department of Computational Biology, St. Jude Children's Research Hospital, Memphis, TN, 38105, USA

[12] Center for Applied Bioinformatics, St. Jude Children's Research Hospital, Memphis, TN, 38105, USA

[13]Institute of Medical Genetics, Wolfson Medical Center, Holon 58100, Israel

[14]Fetal Neurology Clinic, Pediatric Neurology Unit, Wolfson Medical Center, Holon 58100, Israel

[15]Sackler School of Medicine, Tel-Aviv University, Tel-Aviv, Israel

[16]Departments of Pediatrics and Neurology, University of Colorado School of Medicine, Aurora, CO 80045, USA

[17]Amsterdam UMC, University of Amsterdam, Department of Human Genetics, Amsterdam Reproduction and Development Research Institute, Meibergdreef 9, 1105 AZ Amsterdam, Netherlands

[18]Telethon Institute of Genetics and Medicine, Pozzuoli, Italy

[19]Department of Translational Medicine, Federico II University of Naples, Naples, Italy

[20]Department of Medical Genetics, Member of the ERN EpiCARE, University Hospital of Lyon and Claude Bernard Lyon I University, Lyon France

[21]Pathophysiology and Genetics of Neuron and Muscle (PNMG), UCBL, CNRS UMR5261 - INSERM U1315, Lyon, France

[22]Manchester Centre for Genomic Medicine, United Kingdom

[23]Montpellier University, Reference Center for Rare Disease, Medical Genetic Department for Rare Disease and Personalize Medicine, Inserm Unit 1183, CHU Montpellier, Montpellier, France

[24]Neuroscience Research Australia (NeuRA), Sydney, Australia

[25]Prince of Wales Clinical School, Faculty of Medicine, University of New South Wales, Sydney, Australia

[26]New South Wales Health Pathology Randwick Genomics, Prince of Wales Hospital, Sydney, Australia

[27]Centre for Clinical Genetics, Sydney Children's Hospital, Sydney, Australia

[28]Greenwood Genetic Center, Greenwood, SC, 29646, USA

[29]Department of Molecular and Human Genetics, Baylor College of Medicine, Houston, TX 77030, USA

[30]Texas Children's Hospital, Genetic Department, Houston, TX 77030, USA

[31]Department of Pediatrics, Section of Neurology and Developmental Neuroscience, Baylor College of Medicine, Houston, TX 77030, USA

[32]Cain Pediatric Neurology Research Foundation Laboratories, Jan and Dan Duncan Neurological Research Institute, Texas Children's Hospital, Houston, TX, USA, 77030

[33]Texas Children's Hospital, Houston, TX 77030, USA

[34]Department of Neuroscience, Baylor College of Medicine, Houston, TX 77030, USA

[35]McNair Medical Institute, The Robert and Janice McNair Foundation, Houston, TX 77030, USA

[36]Ken and Ruth Davee Department of Neurology, Northwestern University Feinberg School of Medicine, Chicago, IL, USA

[37]Department of Epidemiology and Cancer Control, St. Jude Children's Research Hospital, Memphis, TN 38105, USA

[38]Department of Laboratory Medicine and Pathology, University of Washington, Seattle, WA 98195, USA

[39]Brotman Baty Institute for Precision Medicine, University of Washington, Seattle, WA 98195, USA

[40]Department of Paediatrics, University of Melbourne, Royal Children's Hospital, Melbourne, Australia

[41]Florey Institute and Murdoch Children's Research Institute, Melbourne, Australia

90

91 *These authors contributed equally.

92 #Correspondence: Heather.Mefford@stjude.org and Bekim.Sadikovic@lhsc.on.ca

93

94 **Keywords**: DNA methylation, unsolved, epilepsy, long-read sequencing, nanopore

ABSTRACT

Sequence-based genetic testing currently identifies causative genetic variants in ~50% of individuals with developmental and epileptic encephalopathies (DEEs). Aberrant changes in DNA methylation are implicated in various neurodevelopmental disorders but remain unstudied in DEEs. Rare epigenetic variations ("epivariants") can drive disease by modulating gene expression at single loci, whereas genome-wide DNA methylation changes can result in distinct "episignature" biomarkers for monogenic disorders in a growing number of rare diseases. Here, we interrogate the diagnostic utility of genome-wide DNA methylation array analysis on peripheral blood samples from 516 individuals with genetically unsolved DEEs who had previously undergone extensive genetic testing. We identified rare differentially methylated regions (DMRs) and explanatory episignatures to discover causative and candidate genetic etiologies in 10 individuals. We then used long-read sequencing to identify DNA variants underlying rare DMRs, including one balanced translocation, three CG-rich repeat expansions, and two copy number variants. We also identify pathogenic sequence variants associated with episignatures; some had been missed by previous exome sequencing. Although most DEE genes lack known episignatures, the increase in diagnostic yield for DNA methylation analysis in DEEs is comparable to the added yield of genome sequencing. Finally, we refine an episignature for *CHD2* using an 850K methylation array which was further refined at higher CpG resolution using bisulfite sequencing to investigate potential insights into *CHD2* pathophysiology. Our study demonstrates the diagnostic yield of genome-wide DNA methylation analysis to identify causal and candidate genetic causes as ~2% (10/516) for unsolved DEE cases.

KEYWORDS: DNA methylation; epivariant; episignature; molecular diagnostics; developmental and epileptic encephalopathies

INTRODUCTION

The developmental and epileptic encephalopathies (DEEs) are the most severe group of epilepsies, defined by frequent epileptiform activity associated with developmental slowing or regression[1]. While each genetic etiology is rare, with more than 825 genes implicated[2], the cumulative incidence of DEEs overall is 1 in 590 children[3]. Currently, *de novo,* X-linked, or recessively inherited pathogenic germline variants are found in ~50% of individuals with DEEs who undergo genetic testing[4]. These are identified by gene panels, exome sequencing (ES), and now, genome sequencing (GS)[5-7]. A smaller subset is explained by copy number variants (CNVs)[8]. Understanding the etiology guides management, such as clinical trial participation, informs accurate reproductive counseling, enables families to join gene-based support groups, and facilitates the development of targeted therapies[9-12]. This, in turn, improves outcomes but is not possible when the etiology is unknown ("unsolved").

Epigenetic modifications, which alter the DNA without changing the DNA nucleotide sequence, determine the etiology of some individuals with neurodevelopmental disorders but have not yet been studied in the DEEs. DNA methylation is an essential epigenetic modification that regulates cellular gene expression by adding a methyl (CH_3) group to a DNA strand, typically at CpG sites. This can occur through methylation of promoter CpGs, genomic imprinting, and X-chromosome inactivation[13]. Rare epigenetic variations ("epivariants") disrupt normal methylation and cause disease. While DNA methylation does not change the DNA sequence itself, epivariants are often perpetrated by underlying in-cis DNA changes, such as rare sequence variants, structural alterations, and CG-rich repeat expansions[14] that are difficult to identify by standard sequencing. One example is the methylation of the 5' untranslated region (5'UTR) of *FMR1* (MIM:309550) that represses gene expression and causes Fragile X syndrome (MIM:300624). Similarly, hypermethylation of the 5'UTR of Xylosyltransferase 1 (*XYLT1*, MIM:608124), leading to gene silencing, may identify the "missing" allele in the recessive disease Baratela-Scott

144 syndrome (BSS [MIM:615777])[15]. In both Fragile X and BSS, the aberrant methylation is due to
145 the expansion of a CG-rich repeat that is difficult to reliably detect using short-read sequencing.
146 Rare epivariants, also called rare differentially (hyper- and hypo-) methylated regions (DMRs),
147 are enriched in individuals with neurodevelopmental disorders and congenital anomalies (ND-CA)
148 compared to controls[16].

149 In contrast to rare DMRs, which represent discrete genomic regions with outlier
150 methylation changes, genome-wide epigenetic profiles identify a collection of distinct individual
151 CpG site methylation changes across the genome. A growing number of rare diseases exhibit
152 these methylation patterns, or episignatures, that are reproducible among individuals with
153 pathogenic variants within the same protein domain, gene, or protein complex, yielding highly
154 sensitive and specific biomarkers[17,18]. Since episignatures in diagnostics were first clinically
155 validated and implemented with the EpiSign™ assay in 2019[19], episignatures for nearly 70 rare
156 diseases have been published. Episignatures provide strong evidence for genetic diagnosis,
157 regardless of whether an underlying pathogenic DNA variant is identified, and to resolve variants
158 of uncertain significance (VUS). Episignatures have been found for neurodevelopmental
159 disorders where epilepsy is part of the phenotype, but the diagnostic yield for DEEs has not been
160 determined. Furthermore, how these clinically relevant episignatures might be harnessed to
161 inform underlying disease biology and give insights into potential distinct and overlapping
162 pathogenic mechanisms among disorders is just beginning to be explored[20].

163 Both rare DMRs and episignatures can be detected in peripheral blood samples. Rare
164 DMRs derived from individuals with ND-CA are recapitulated across multiple tissue types,
165 including blood and fibroblasts[16]. Episignature classifiers are trained on data obtained from blood-
166 derived DNA and are, therefore, blood-specific.

167 Here, we assessed rare outlier DMRs and DNA methylation episignatures in peripheral
168 blood-derived DNA from 516 individuals with genetically unsolved DEEs. We report our

methylation array data processing pipeline, MethylMiner, which automates quality control, normalization, and implementation of an algorithm that mines rare DNA methylation events[14] in addition to interactive data visualization. Using a combination of short- and long-read sequencing (LRS), we identify variants underlying rare epivariants and episignatures. Finally, we refine the robust episignature for the DEE gene *CHD2* (MIM:602119)[18] to explore how clinically relevant episignatures may give insights into underlying biology. For individuals with unsolved DEEs, we show that rare epivariants and episignatures uncover molecular causes missed using standard sequence-based approaches.

MATERIALS AND METHODS

Cohorts

Our cohorts consist of 530 affected individuals (43% female) with unsolved DEEs and 478 healthy controls (46% female) (Figure S1, Table S1, Supplemental Methods). An additional 146 analytical controls (60% female) were included for validation. Individuals with DEEs were recruited from investigators' research and clinical programs[21,22]. Methylation array data for healthy controls were drawn from a public database[23] (n=111), an internal institutional database (n=337), and 30 unaffected parents of probands with DEEs (Supplemental Methods). Eight family members with epilepsy were studied to identify familial methylation patterns (shared rare DMRs or episignatures). Analytical controls, including i) six individuals each with a disease-associated rare DMR, ii) 24 individuals with a pathogenic variant in a gene or CNV associated with an episignature, and iii) 116 individuals with a pathogenic variant in a gene without a known episignature, were used to validate positive and negative rare DMR and episignature findings in the DEE cohort. After quality control and normalization (described below), there were 516 remaining individuals with unsolved DEEs who had undergone extensive molecular testing: 80%

had a gene panel, 40% microarray analysis, 76% ES, and 38% GS. Collectively, 98% had at least one sequence-based investigation (gene panel, ES, or GS). There were also 464 healthy controls, 141 analytical controls, and eight affected family members for DNA methylation analysis. This study was approved by the Institutional Review Board (IRB) of St. Jude Children's Research Hospital (SJCRH). Written informed consent was provided by parents or legal guardians of individuals with DEEs with local IRB approval from SJCRH, Austin Health (Australia), the University of Washington (UW), and the National Institutes of Health (NIH).

Methylation Array

All data were derived from peripheral blood-derived DNA, except for five analytical control samples used for outlier DMR analysis: saliva-derived DNA from one female individual with BSS and her parent and lymphoblastoid cell line (LCL)-derived DNA from three individuals, including two males and one female, with Fragile X syndrome (Coriell). These samples were used as positive controls to validate the outlier analysis, and then removed from the final analysis to minimize potential cell type differences. DNA was extracted from peripheral blood samples using standard protocols, with approximately 250-500ng of DNA bisulfite converted. The Illumina Infinium MethylationEPIC v1.0 (850K array) bead chip arrays (processed according to the manufacturer's protocol, Supplemental Methods) interrogate >850,000 individual CpG sites, including CpG islands, promoter regions, gene bodies, FANTOM5 enhancers, and proximal ENCODE regulatory elements[24].

Of 1,162 individuals included, three individuals were run in triplicate, and 29 were run in duplicate across different batches to produce a total of 1,197 blood-derived DNA methylation array samples before quality control and processing. Each sample consisted of data for >850,000 probes that were rigorously quality-controlled for the removal of outlier samples as opposed to

outlier regions of interest. All data were combined and loaded into the R package minfi[25] for quality control and normalization and the R package SVA[26] for batch correction using the ComBat method[27]. Individual CpG probes that failed (detection p>0.01) in >10% of samples and probes overlapping with common SNPs were removed. Samples judged to be of poor quality (>1% of probes that failed) and samples that were deemed outliers based on manual inspection of the principal component analysis (PC1 and PC2), using β values for probes located on chromosome (chr) 1, were removed. We estimated blood cell type composition for six cell types (CD8T, CD4T, NK, B-cell, monocytes, and granulocytes) from β values for each sample[28]. Samples containing outlier cellular fractions defined as ≥99th percentile +2% or ≤1st percentile -2% for at least two of the six cell types were also removed. Methylation array intensity values on the sex chromosomes (X, Y) were used to infer the sample sex and compared to the clinically reported sex. Samples with sex mismatch were removed. Samples were separated into inferred sex (males and females) for all downstream analyses of sex chromosomes. This quality control and filtering left 1,161 samples across 1,129 individuals (26 individuals in duplicate and three individuals in triplicate across batches) assayed by the 850K array and 833,834 probes (814,945 autosomal probes and 18,889 sex chromosome probes) (Table S1).

Identification and Annotation of Rare Epivariants

To identify outlier DMRs, we used a sliding window approach as previously described[14]. In brief, this algorithm employs user-defined quantile thresholds to determine outlier β values across multiple CpG sites. Per 1Kb window, at least three consecutive CpG sites must exhibit outlier β values in the same direction (hyper or hypo) for a sample compared to the rest of the cohort to be considered an outlier DMR. We considered β values above the 99.25th percentile plus 0.15 as hypermethylated, and those below the 0.75th percentile minus 0.15 as hypomethylated for analysis of the autosomes (chr1-chr22). Since samples were split into inferred sex (males and

females) for analysis of the sex chromosomes, the stringency was adjusted accordingly to 99th plus 0.15 for hypermethylated and 1st percentile minus 0.15 for hypomethylated. DMRs were then annotated to inform functional interpretation using HOMER[29] and including overlap with UCSC RefSeq gene bodies and promoter regions, defined as ±2Kb of the transcription start sites (TSS), known CpG islands (CGIs), repetitive-element information (RepeatMasker and SimpleRepeats), imprinting control centers[30], CTCF-binding sites[31], gene molecular function information[29], OMIM phenotype[32], average brain expression using bulk RNA-seq data from the GTEx Portal, and in-house epilepsy- and candidate-gene lists to prioritize candidates but not as exclusion criteria. Additionally, a recent study delineated the rare DMR landscape in the human population by examining 450K methylation array data from >23,000 individuals[14]. Regions from those data were checked against our DMRs where possible to determine the frequency at which each DMR occurs in the population. Based on this annotation information, DMRs were prioritized by four features: (1) a low or negligible population frequency; (2) a well-annotated genomic location, such as in or near known epilepsy and candidate genes; (3) recurrence in multiple individuals; and (4) manual inspection of DMRs, including flanking regions.

Development of a DNA Methylation Array Analysis and Visualization Pipeline

We developed MethylMiner, a methylation array analysis pipeline tailored toward discovering rare epivariants with interactive data visualization. The pipeline requires standard input files, raw signal .idat files containing each sample's green and red channels, and a metadata sheet including sample names, sentrix IDs, reported sample sex, and sample group (if applicable). In brief, the pipeline performs quality control and normalization as described to derive output files, including quality control reports, β values, M-values, and bigWig files for quick and convenient visualization in the integrative genomics viewer (IGV)[33]. The pipeline then performs the outlier DMR analysis (using scripts derived from: https://github.com/AndyMSSMLab/Methylation_script) based on user-

defined quantile thresholds and outputs the DMRs and annotations into a tabulated sheet. This annotated list of DMRs is then used as input for the interactive data visualization in JupyterDash, which allows users to interact with plots for quality control metrics, DMR annotations, and DMR genomic tracks. The pipeline is hosted on our GitHub page (https://github.com/stjude-biohackathon/MethylMiner).

Validation of Outlier DMRs Using Enzymatic Methyl-Sequencing

We performed targeted Enzymatic Methyl-sequencing (targeted EM-seq) enriched with the Twist Human methylome panel targeting 3.98M CpGs through 123 Mb of genomic content. Targeted EM-seq of peripheral blood-derived DNA was used to validate a subset of outlier DMRs, including n=2 positive control DMRs (*XYLT1* and *FMR1*) and n=29 DMRs-of-interest called amongst n=3 individuals with unsolved DEEs. EM-seq library preparation, target enrichment, and sequencing were performed using standard protocols[34]. Reads were processed using the "nf-core/methyseq" pipeline with the '--emseq' flag. For detailed EM-seq methods, please refer to Supplemental Methods.

Identification of Structural Variants with Long-Read Sequencing

We used both targeted and whole-genome LRS on the Oxford Nanopore Technologies (ONT) platform to validate rare DMRs and identify candidate disease-causing variants at or near the site of interest (Table S2A). Targeted LRS using the "read-until" function was performed on an ONT GridION using a single R9.4.1 flowcell as described previously[35]. At least 100Kb of sequence was added to either side of the target region for capture. Libraries for GS were prepared using the ligation sequencing kit (SQK-LSK110) following the manufacturer's instructions, then loaded onto a single flowcell (FLO-PRO110, R9.4.1) on a PromethION and run for 72 hours with one wash

and reload. All data were base called using Guppy 6.3.2 (ONT) with the superior model including 5mC methylation. Reads were aligned to GRCh38/hg38 using minimap2[36], SNP and indel variants were called using Clair3[37], structural variants were called using Sniffles[38], SVIM[39], and CuteSV[40], and phasing was performed using LongPhase[41]. Aligned and phased bam files were visualized in IGV[33].

Episignature Testing

Data were blinded and submitted to the clinical bioinformatics laboratory [Molecular Diagnostics Laboratory, London Health Sciences Centre (LHSC), Western University, London, Canada] through a secure file transfer protocol and stored on encrypted servers. DNA methylation data for each sample were compared to clinically validated DNA methylation episignatures for all disorders which are part of the EpiSign™ v4 clinical test[42]. The reference database EpiSign™ Knowledge Database (EKD) includes thousands of clinical, peripheral blood DNA methylation profiles from disorder-specific reference and normal controls (general population samples of various ages and racial backgrounds). Individual DNA methylation data for each individual were compared with the EKD using the support vector machine (SVM) based classification algorithm for EpiSign™ disorders. A Methylation Variant Pathogenicity (MVP) score between 0 and 1 was generated to represent the confidence of prediction for the specific disorder the SVM was trained to detect. Conversion of SVM decision values to these scores was carried out according to the Platt scaling method[43].

Classification for a specific EpiSign™ disorder included a combination of MVP score, hierarchical clustering, multidimensional scaling (MDS) of an individual's methylation data relative to the disorder-specific EpiSign™ probe sets and controls. MVP score assessment had a scale with thresholds of >0.5 for positive, <0.1 negative, 0.1–0.5 inconclusive or moderate confidence.

A detailed description of this analytics protocol was described previously[18,44]. Possible types of results included: positive (matching an EpiSign™ disorder), negative (not matching any EpiSign™ disorder), and inconclusive (described in detail in results).

Exome and Genome Sequencing

If sequencing data were already available for the individual on a collaborative research basis, these data were reviewed. If the data were unavailable, ES or GS was performed on peripheral blood-derived DNA using standard Illumina short-read sequencing techniques and bioinformatic approaches (Supplemental Methods). We validated potentially pathogenic variants with Sanger sequencing and confirmed sample identity and relatedness (e.g. trios) using Powerplex Short-Tandem Repeat (STR) Identification analysis.

RNA-sequencing and Gene Expression Analysis

RNA was extracted from dermal fibroblasts established from skin punch biopsies for Family 2 (n=2) and Family 3 (n=3) described in the results. RNA-seq was performed using standard Illumina short-read sequencing practices (Supplemental Methods), and the reads were processed using the "nfcore/rnaseq" pipeline. Removal of the adapter sequences was performed using Trim Galore!, and low-quality reads were eliminated with FastQC[45]. Subsequently, reads were aligned to a reference genome using the STAR aligner[46]. Gene expression quantification was performed using Salmon[47], which estimates transcript abundance. To determine gene "dropout," the OUTRIDER algorithm[48] was applied to RNA-seq data for Family 2 (proband and parent), Family 3 (proband and parent 2), and Family 3 (parent 1 and parent 2) against a publicly available dataset of n=139 fibroblast samples[49]. PCA displayed no batch groupings, and genes with Fragments Per

Kilobase of transcript per Million mapped reads (FPKM)<1 were removed as lowly expressed genes. Results were considered significant if they had a *padj*<0.05 and a z-score cutoff of ±2.

Refinement of a CHD2 Episignature

A total of 17 females and 12 males with genetic variants in *CHD2* and clinical features consistent with *CHD2*-epileptic encephalopathy of childhood (EEOC) were included in this expanded 850K cohort. The detailed list of genetic variants classified as pathogenic or likely pathogenic according to the American College of Medical Genetics guidelines is in Table S2B. All samples and records were deidentified.

Details of the methylation data analysis and episignature refinement are as previously described[18,50-52]. Briefly, methylation signal intensities were imported into R 4.1.3 for analysis. Normalization was performed by the Illumina normalization method with background correction using minfi[25]. Probes located on X and Y chromosomes, known SNPs, or probes that cross-react (as reported by Illumina) were excluded. Samples containing failed probes of more than 5% (p>0.1, calculated by the minfi package) were also removed. The genome-wide methylation density of all samples was examined, and principal component analysis (PCA) was performed to visualize the overall data structure of the batches and to identify outlier samples. All 29 samples passed and were used for probe selection. The MatchIt package was used to randomly select controls, which were matched for age, sex, and array type from the EKD at the LHSC, as previously described[18,53]. The methylation level of each probe was calculated as the ratio of methylated signal intensity over the sum of methylated and unmethylated signal intensities (β-values), ranging between 0 (completely unmethylated) and 1 (fully methylated). β-values were then converted to M-values by logit transformation using the formula $\log_2(\beta/(1-\beta))$ to perform linear regression modeling, which was used to identify the differentially methylated probes (DMPs), via the R package limma[54]. The analysis was also adjusted for blood cell-type compositions, using

the Houseman algorithm[55]. The estimated blood cell proportions were added to the model matrix of the linear models as confounding variables. The generated *p*-values were moderated using the eBayes function in the limma package and were corrected for multiple testing using the Benjamini and Hochberg (BH) method.

Following this, probe selection was performed in three steps. Firstly, 1000 probes were selected, which had the highest product of methylation difference means between case and control samples and the negative of the logarithm of multiple-testing corrected *p* values derived from the linear modeling. Secondly, a receiver's operating characteristic (ROC) curve analysis was performed, and 200 probes with the highest area under the ROC curve (AUC) were retained. Lastly, probes having pair-wise Pearson's correlation coefficient greater than 0.85 within case and control samples separately were removed (none of the selected 200 probes met this criteria). This resulted in the identification of 200 DMPs. These probes were used for the construction of a hierarchical clustering model using Ward's method on Euclidean distance, as well as a MDS model by scaling of the pairwise Euclidean distances between samples.

Functional Annotation and Correlation of the *CHD2* Episignature

Functional annotation and episignature cohort comparisons were performed according to our published methods[44]. Briefly, to assess the percentage of DMPs shared between the CHD2 episignature and other neurodevelopmental conditions on the EpiSign™ clinical classifier, heatmaps and circos plots were produced. Heatmaps were plotted using the R package pheatmap (version 1.0.12) and circos plots using the R package circlize (version 0.4.15)[56]. To determine the genomic location of the DMPs, probes were annotated in relation to CGIs and genes using the R package annotatr[57] with AnnotationHub and annotations hg19_cpgs, hg19_basicgenes, hg19_genes_intergenic, and hg19_genes_intronexonboundaries. CGI annotations included CGI shores from 0–2Kb on either side of CGIs, CGI shelves from 2–4Kb on either side of CGIs, and inter-CGI regions encompassing all remaining regions. A chi-squared

goodness of fit test was performed in R to investigate the significance between background DMP annotation distribution and the CHD2 cohort annotation distribution. *P* values were obtained for both annotation categories (gene and CGIs). To assess the relationship between the expanded 850K only CHD2 cohort and other EpiSign™ disorders, the distance and similarities between cohorts were analyzed using clustering methods and visualized on a tree and leaf plot. This assessed the top 500 DMPs for each cohort, ranked by *p*-value. For cohorts with less than 500 DMPs, all DMPs were used. Tree and leaf plots, generated using the R package TreeAndLeaf[58], illustrated additional information, including global mean methylation difference and total number of DMPs identified for each cohort.

Whole-Genome Bisulfite Sequencing

Genomic peripheral blood-derived DNA from n=3 CHD2 trios (proband and parents) and n=1 CHD2 singleton (proband) (total n=10 samples) were bisulfite-converted and then underwent whole-genome bisulfite sequencing (WGBS) using standard Illumina short-read sequencing processing methods (Supplemental Methods). Reads were trimmed by Trim Galore! and aligned to the GRCh38/hg38 human genome reference using BSMAP2.74. The methylation ratios from BSAMP mapping results were extracted using methratio.py. Duplicated reads were removed and CpG methylation from both strands was combined. The methylation ratios were also corrected according to the C/T SNP information estimated by the G/A counts on reverse strand.

DMR Calling of DNA Methylation Array and WGBS

We performed DMR analysis on Illumina 850K EPIC methylation array data for 16 individuals with DEEs harboring pathogenic variants in *CHD2* compared to 18 controls. The data were normalized using the minfi package's functional normalization algorithm[59], and we employed two independent R packages to call DMRs, bumphunter[60] and DMRcate[61]. DMRs were defined as those passing

a significance threshold of $p<0.05$ for bumphunter and Fisher's multiple comparison $P<0.05$ for DMRcate. A minimum of three CpGs and mean methylation difference between CHD2 and controls of at least 5% was also required (bumphunter "cutoff" and DMRcate "betacutoff"=0.05) in either the hyper or hypo direction. For bumphunter, smoothing was used, and the number of permutations for each condition was set to B=1000. For DMRcate, default settings were used, and the Gaussian kernel bandwidth for smoothed-function estimation was set to λ=1000, meaning that significant CpGs further than 1000 nucleotides were in separate DMRs.

The methylCall data from WGBS, which consists of the total number of reads covered for each CpG site and the number of methylated C's at each CpG site, was used for calling DMRs between four individuals with DEEs caused by pathogenic *CHD2* variants and six unaffected parents. Firstly, CpG sites with less than 10X coverage and those on the sex chromosomes were removed. DMRs were called from WGBS methylCall data using two independent R packages, DMRcate[62] and DSS[63]. DMRcate identifies and ranks the most differentially methylated regions across the genome, while DSS detects differentially methylated loci or regions from WGBS. For DMRcate, the scaling factor for bandwidth "C" was set to 50, as recommended for WGBS. DSS was run with default parameters. DMRs were defined by each algorithm (with smoothing) as regions of a minimum of five CpGs with significance (Fisher's multiple comparison *P* value <0.05) and minimum methylation differences of 5% in either the hyper or hypo direction (DSS "delta" and DMRcate "betacutoff"=0.05) between cases and controls.

The genomic locations of output DMR calls were intersected between both callers requiring a minimum overlap of 50bp in the same direction to reduce the false positive rate. This resulted in high-confidence list of DMRs predicted by two independent callers for array (bumphunter and DMRcate) and WGBS (DMRcate and DSS). The methylation difference between CHD2 and control was averaged between both callers for the final DMR list. DMRs were segmented by mean methylation difference between CHD2 and control (5%, 10%, 15%, and 20%) for visualization and annotation with CpG elements (islands, shores, shelves) and gene regions

(1-5Kb upstream TSS, promoters as <1Kb upstream TSS, 5'UTRs, exons, introns, and 3'UTRs) using annotator[57]. To get adequate CpG element counting (i.e. a DMR spanning both a shore and shelf would not get counted twice), CpG annotations were adjusted for DMR size by calculating representation across CpG elements as a fraction of the total DMR length.

RESULTS

Discovery and Validation of DMRs in Unsolved DEEs

To determine the ability of our analysis pipeline to robustly detect rare, outlier DMRs, we included DNA from six positive controls with genetic diseases: three individuals with heterozygous or homozygous hypermethylation of *XYLT1*, and three individuals (two males and one female) with hypermethylation of *FMR1*. The outlier DMR analysis detected both rare DMRs (Figure S2, Table S3A). Additionally, we identified an *XYLT1* heterozygous hypermethylation carrier in our DEE cohort. Targeted X-chromosome analysis in males identified complete methylation at the *FMR1* locus in both Fragile X males compared to the remaining cohort, all of which were completely unmethylated at *FMR1*. *FMR1* hypermethylation was also higher (~75%) in the Fragile X female sample compared to the other females with 25-50% methylation, likely due to random X-inactivation. Thus, our methylation array analysis approach detects outlier DMRs at known disease loci for the autosomes and sex chromosomes.

Next, we assessed outlier DMRs in our cohort of 1,124 individuals (516 unsolved DEE) across 1,156 array samples. We predicted n=2,140 total DMRs for the autosomes, n=59 DMRs for males on chromosome X, n=42 DMRs for females on chromosome X, and no DMRs on chromosome Y (Table S3B, S3D, S3F). After accounting for DMRs overlapping across samples (≥50% probe overlap in the same direction of DNA methylation hyper- or hypo-methylation), we derived n=1,540 unique DMRs for the autosomes (917 hyper, 623 hypo), n=45 for males on chrX (26 hyper, 19 hypo), and n=34 for females on chrX (20 hyper, 14 hypo) (Table S3C, S3E, S3G).

Of the samples with one or more outlier DMRs, the majority had only a single outlier DMR (Figure S3).

To determine the robustness of our DMR calling algorithm, we (i) assessed the reproducibility of DMR calls in a subset of samples and (ii) performed validation of DMRs using targeted EM-seq (Supplemental Methods). Using replicate array data for 29 individuals, we found that 80% of DMRs were replicated across different batches for an individual (Supplemental Methods). We then used targeted EM-seq, a non-bisulfite approach, to validate a subset of DMRs. We confirmed that our positive control DMRs (*XYLT1* and *FMR1*) could be detected in the targeted EM-seq data (Figure S4). We then validated 30 outlier DMRs by targeted EM-seq in four individuals with unsolved DEEs (Figure S5 and S6). In addition to DMR validation, targeted EM-seq provides much higher resolution of the extent of differential methylation than the methylation array (e.g. >100 methylated CpG sites for the *XYLT1* DMR by targeted EM-seq compared to eight representative probes on array; Table S4). Thus, we detected and validated outlier DMRs at higher resolution using an orthogonal approach.

Rare Outlier DMRs in Unsolved DEEs

We narrowed down outlier DMR calls for individuals with unsolved DEEs to determine high-priority candidates for further study based on DMR recurrence across multiple individuals, population frequency[14], functional annotations (Methods), and manual inspection of DMR plots for each DMR. We identified 11 individuals with unsolved DEEs with one or more rare, potentially disease-associated DMRs and performed follow-up studies (Table 1, Table S2A). One individual had multiple DMRs due to a balanced translocation between chrX and chr13, four individuals had a DMR due to expanded CG-rich repeats, and six individuals had DMRs due to underlying CNVs.

Rare Outlier DMR Analysis Detects Hypermethylation of chr13 Due to X;13 Translocation

One female with the DEE syndrome, epilepsy of infancy with migrating focal seizures (EIMFS), had 27 rare outlier hypermethylated DMRs across chr13 (Figure 1A, Figure S7), none of which were present in >23,000 controls[14]. The DMRs were replicated on a second, independent methylation array from the same individual and validated using targeted EM-seq (Figure S6). Methylation array analysis of both parents revealed that all rare hypermethylated DMRs occurred *de novo* in the proband (Figure 1B). Whole-genome ONT long-read sequencing also confirmed the hypermethylated DMRs and identified a balanced translocation between chrX and chr13 (Figure 1C), annotated as 46,XX,t(X;13)(q28;q14.2). The translocation provides a mechanism whereby random X-inactivation induces hypermethylation on the portion of chr13q attached to the large piece of the X chromosome. The translocation breakpoints were confirmed by PCR and Sanger sequencing of peripheral blood-derived DNA as chrX:152,092,342 to chr13:47,005,269 and chr13:47,005,271 to chrX:152,092,344 (GRCh38/hg38). Parental methylation studies and short-read GS confirmed that the translocation occurred *de* novo. The translocation is likely causative in this individual given the *de novo* occurrence, absence of clearly pathogenic sequence variants by trio sequence (Table S5), and report of a similar translocation in a female individual with intellectual disability and bilateral retinoblastoma[64].

Rare Outlier DMR Analysis Detects Hypermethylation Caused by Underlying Triplet Repeat Expansions

We detected two individuals with unsolved DEEs and one control individual with hypermethylation spanning the 5'UTR and intron 1 of the Casein kinase 1 isoform epsilon (*CSNK1E*, MIM:600863, Figure 2A) gene. Although present in one control and reported in 6/23,116 controls[14], an individual with DEE and probable haploinsufficiency due to a *de novo* splicing variant (c.885+1G>A) in

513 *CSNK1E* has been reported[65], suggesting further study is warranted to determine if variation in
514 this gene causes DEE. Segregation analysis revealed that the hypermethylation in one proband
515 was inherited (Family 1, Figure S8), whereas the other arose *de novo* (Family 2). After validation
516 of hypermethylation with targeted EM-seq for both probands (Figure S5), long-read sequencing
517 of the proband (whole-genome) and parent (targeted) from Family 1 confirmed the presence of
518 an expanded CGG motif in both (Figure 2B), as previously reported in individuals with
519 hypermethylation of *CSNK1E* at fragile site FRA22A and reduced expression in lymphoblastoid
520 cells[14]. Through GeneMatcher[66], we identified Family 3 consisting of a proband with the same
521 *CSNK1E* hypermethylated DMR inherited from his parent, who is mildly affected by learning,
522 speech, and sleep difficulties (Supplemental Phenotype data). Expression analysis in available
523 fibroblasts from Families 2 and 3 showed that individuals with *CSNK1E* hypermethylation had
524 decreased expression of *CSNK1E* compared to hypermethylation-negative controls (Figure 2C).
525 Analysis using the OUTRIDER algorithm[48] confirmed "drop-out" of *CSNK1E*
526 (ENSG00000213923) expression compared to publicly available fibroblast controls[49] (Figure 2C,
527 Figure S9). Thus, we report 3 individuals with unsolved DEEs harboring inherited and *de novo*
528 *CSNK1E* hypermethylation due to an underlying repeat expansion (n=4 LRS) that leads to
529 approximately 50% reduction in *CSNK1E* expression (n=3 RNA-seq drop-out). No other
530 candidate gene variants for these 3 probands were found by trio GS analysis. However, due to
531 finding this abnormality in seemingly unaffected individuals, one control and one parent (Family
532 1) in our cohort and others[14], further work is required to determine whether variations in *CSNK1E*
533 cause or contribute to the DEEs.

534 A male individual with unsolved DEE displayed inherited hypermethylation of the *DIP2B*
535 (MIM:611379) promoter region and exon 1 (Figure S10), which is due to an underlying CGG-
536 repeat expansion and fragile site FRA12A[67]. Loss of *DIP2B* is associated with an autosomal

dominant neurodevelopmental disorder (NDD) with variable penetrance, including a *DIP2B* repeat expansion in an individual with epilepsy[67].

We detected a rare hypermethylated DMR on the X chromosome in exon 1 of an uncharacterized gene (*BCLAF3/CXorf23*) in a male with unsolved DEE (Figure S10), that was absent in >23,000 unaffected controls (>8,000 males)[14]. We validated hypermethylation using targeted EM-seq (Figure S5), and ONT long-read sequencing of the proband and his parent revealed a novel CGG repeat expansion in the proband (~2,500-3,000bp, Figure S11) inherited from his parent, who had a smaller expansion (~1,700-1,900bp). LRS and standard X-inactivation studies[68] show that the parent has skewed X-inactivation (Table S6) of the allele with the expansion, which explains why outlier hypermethylation is not detected from her methylation array data. There are no other candidate variants for the proband's DEE by trio GS. Collectively, these results highlight the detection of repeat-expansion-associated loci based on outlier DMR analysis of DNA methylation array in individuals with unsolved DEEs.

Rare Outlier DMR Analysis Detects Copy Number Variants

Six individuals displayed DMRs that were found to be due to underlying CNVs. One control and an individual with unsolved DEE had ~10-15 hypomethylated DMRs along chr2 spanning ≥144Kb (Figure S12A). Short and long-read sequencing analysis revealed this "DMR" was due to a homozygous ~182Kb deletion encompassing outlier DMRs (Figure S12C). Segregation testing found that the proband inherited the deletion from both parents, who were heterozygous carriers. The CNV was also found on DNA methylation array using the R tool conumee[69] (Figure S12B).

Four individuals with unsolved DEEs and one control had a 686bp hypomethylated DMR in intron 2 of the gene *LINGO1* (MIM:609791). DNA methylation array analysis for a proband's parent found that the hypomethylation was at least in part inherited, and short and long-read

sequencing revealed that hypomethylation was caused by an underlying ~4Kb inherited deletion (Figure S13).

Another individual with unsolved DEE had hypermethylation in the 5'UTR of *CFAP36*/*CCDC104* (Figure S14A), which was not present in >23,000 controls[14]. DNA methylation array analysis of both parents indicated it was inherited (Figure S14B), and targeted ONT long-read sequencing revealed a ~500Kb tandem duplication from chr2:55,034,228-55,536,971 (GRCh38/hg38). Collectively, these results indicate that outlier DNA methylation can be due to underlying CNVs and that the 850K methylation array may not have sufficient coverage to detect smaller CNVs. Due to the high population frequencies and inheritance status of the CNVs we found, we determined they are unlikely to contribute to the individuals' phenotypes. Still, these findings illuminate ways in which detected DNA methylation changes are influenced by underlying DNA variation.

Episignature Screening Validates Pathogenicity of Genetic Diagnoses and Resolves Variants of Uncertain Significance

We next performed episignature analysis, using the EpiSign™ v4 classifier, including 70 conditions associated with 96 genes/genomic regions (Figure 3). To validate our approach, we included several individuals with causal variants in episignature genes or CNVs and an individual with a VUS. These included sixteen individuals with variants in *CHD2* (n=15 pathogenic, n=1 VUS) and one individual each with a pathogenic variant in *KDM5C*, *SETD1B*, *KMT2A*, or *SMARCA2* (Table S2B). We also included two individuals with CNVs, including chr17p11.2 deletion and duplication. Fifteen of the individuals with variants in *CHD2* were positive for the epileptic encephalopathy of childhood (EEOC) episignature[18], also known as the developmental and epileptic encephalopathy 94 (DEE94) episignature. However, one individual with a VUS in

CHD2 was negative for the episignature, and in combination with other clinical evidence the VUS was reclassified as likely benign (Supplemental Phenotype data). The individuals with variants in *KDM5C* (MIM:314690), *SETD1B* (MIM:611055), *KMT2A* (MIM:159555), and *SMARCA2* (MIM:600014) were all positive for the episignatures associated with their disorders. While these individuals were considered solved before episignature screening, the finding was used to support the genetic diagnosis of the individual with a *KDM5C* variant.

Additionally, we identified two individuals with inconclusive results for episignatures despite definitive genetic and clinical findings for the associated syndromes. Inconclusive findings are caused by methylation profiles that partially overlap existing signatures but are not a definitive match. This included an individual with a 17p11.2 deletion inconclusive for the Smith-Magenis syndrome episignature (SMS_del) and a female individual with a 17p11.2 duplication inconclusive for the Potocki-Lupski syndrome episignature (PTLS, Figure S15). In each case, the inconclusive episignature finding is concordant with the genetic diagnosis but yields an inconclusive result potentially attributable to variability introduced by differential CNV breakpoints. Because of this and other factors, inconclusive EpiSign™ results are reported with the caveat that further follow-up or investigation may be warranted if there is a clinical phenotype consistent with the inconclusive episignature in question.

Episignature Screening Solves Genetically Unsolved DEEs

We then tested our cohort of 516 individuals with unsolved DEEs for 70 clinically validated episignatures, leading to a likely diagnosis in five individuals (Table 2). All methylation variant pathogenicity (MVP) scores for episignatures and detailed genomic variant information are in Table S2C. Two unrelated individuals with unsolved DEEs were positive for the KGB syndrome episignature (KGBS_MRD23) caused by pathogenic variants in *ANKRD11* (Figures S16 and

S17). Exome or genome sequencing analysis revealed *de novo* pathogenic stop-gain variants in both individuals, and phenotypes for each individual are consistent with the diagnosis (Supplemental Phenotype data). One proband had affected siblings and family members (n=8, Figure S17). However, none harbored the *ANKRD11* episignature and neither affected sibling harbored the variant, indicating that there is likely a different explanation for this familial epilepsy. One individual with unsolved DEE was positive for the episignature associated with *SETD1B* (Figure S18). Exome sequencing revealed a pathogenic stop-gain variant in *SETD1B*. Another individual with unsolved DEE harbored the episignature for *TET3* and had an inherited pathogenic stop-gain variant in *TET3* on GS (Figure S19). This remains the likely cause of the individual's DEE as the parent has a milder phenotype including macrocephaly and learning difficulties (Supplemental Phenotype data). One male individual with unsolved DEE was positive for the *UBE2A* episignature (Figure S20). Through exome sequencing, we identified a predicted damaging inherited missense variant absent in gnomAD (c.376G>A, p.Ala126Thr). Although the variant does not reach likely pathogenic classification using existing ACMG criteria, the prediction scores (REVEL=.776, CADD=26.4, and PolyPhen-2=1.00) support pathogenicity; the variant is inherited in an X-linked intellectual disability disorder; and the individual shares multiple phenotypic features with *UBE2A* disorder. Thus, the variant has been determined to be the most likely genetic cause of disease.

Of the high-confidence episignature findings, only one individual had an established genetic diagnosis in another gene. This individual harbored a *de novo* variant in *PTEN* with a consistent phenotype of macrocephaly and focal epilepsy but also had the episignature for *KDM2B*. Further analysis identified an inherited missense variant in *KDM2B.* We performed methylation array analysis for the unaffected parent who also harbored the *KDM2B* episignature. This variant is predicted to be likely pathogenic (LP) by ACMG criteria due to its putative effect on splicing regulation, though assessment of this variant with SpliceAI predicts that it does not have

a high likelihood of affecting splicing (Δ score for Donor Gain:0.01). When this criterion is taken away, the designation of LP is reduced to a VUS; other computational predictors assess the impact to be uncertain (REVEL=0.517). Thus, while it is unlikely that this *KDM2B* variant explains the individual's phenotype, it still represents an underlying DNA change detected through episignature screening. Collectively, we have identified positive episignatures and causal genetic etiologies in five previously unsolved individuals with DEEs through episignature screening.

An additional 40 individuals with DEEs (80% unsolved) and nine controls had inconclusive results for episignatures (Figure S20). Of the individuals with DEEs, 4/40 were run across multiple methylation array batches. Three individuals did not reproduce their inconclusive episignature result in the other sample(s). While one individual's inconclusive result did replicate across the different batches, no pathogenic variants were found by GS in the associated genes(s). Of all the individuals with available sequencing data (n=27), none harbored pathogenic variants in the genes associated with episignature findings. While some had overlapping clinical features, most were discordant with the described phenotypes for their inconclusive episignature finding. Additional follow-up will be required to determine whether these inconclusive results are due to array artifacts or have underlying biological or disease-associated meaning. If technical artifacts are ruled out, an inconclusive result may be caused by episignatures in other genes that are yet to be defined and trained against for specificity of the classifier.

Redefining the CHD2 Episignature on the 850K EPIC Array

While episignatures are proven to be clinically useful for diagnosis, little work has been done to investigate how episignatures may inform disease biology by studying DMRs that may impact gene expression. Here, we performed refinement and in-depth analysis of the episignature for the DEE gene *CHD2*. The CHD2 episignature was originally derived using overlapping 450K and

850K DNA methylation array probes representing individual CpG sites in n=9 individuals with pathogenic *CHD2* variants[18]. We refer to this signature as the CHD2 450K episignature (Figure 4A upper, Figure S21A, Table S7). Here, we refine the CHD2 episignature exclusively on 850K EPIC methylation array probes with data from a cohort of n=29 individuals with pathogenic *CHD2* variants (Figure 4A lower, Figure S21B, Table S7). We refer to this signature as the CHD2 850K episignature. Of the 200 probes included in the CHD2 850K episignature, 79/200 are specific to the 850K EPIC array.

Comparison of the CHD2 Episignature to 55 Other Clinically Validated Episignatures

We then compared the CHD2 450K and 850K episignatures to 55 other NDD episignatures (57 total including CHD2)[20] by examining shared probes (Figure 4B, Figure S22), Euclidean clustering (Figure 4C), probe mean methylation differences (Figure S23), and functional annotations (Figure S24). As expected, the CHD2 850K episignature shares the most probe overlap with the CHD2 450K episignature (86/200 or 43%, Figure 4B, Figure S22). Euclidean clustering was used to examine the relatedness of the episignatures by probe overlap and directionality. The CHD2 850K episignature shares the closest branchpoint with the MRXSCJ episignature for *KDM5C* of which it shares 7% of its top 500 DMPs. Collectively, both 450K and 850K episignatures do not share immediate branches (other than the primary branchpoint) with many other episignatures. This may indicate different sets of predominant pathways underlying *CHD2* pathophysiology compared to the other episignatures. Additionally, the CHD2 850K episignature represents more hypermethylated regions than the CHD2 450K episignature, as depicted by the mean methylation differences in Figure 4C and Figure S23. We also performed functional annotation of episignature probes for CpG characteristics and gene regions in relation to the 55 other NDD episignatures (Figure S24). We found that both CHD2 850K and 450K DMPs map to predominately the coding regions of genes (46% and 41%, respectively) with a significant difference in the distribution of

DMPs in these regions compared with the background probe distribution ($P<9.06 \times 10^{-69}$ and $P<2.02 \times 10^{-79}$, respectively). Though the CHD2 850K episignature represents a higher portion of interCGI regions compared with the 450K episignature (43% vs. 31%, respectively), both are enriched in interCGI regions relative to background probe distribution ($P<2.26 \times 10^{-121}$ and $P<9.17 \times 10^{-144}$).

The CHD2 Episignature is Associated with Differentially Methylated Regions

Since *CHD2* encodes a chromatin remodeler that has been shown to regulate gene expression[70,71], we investigated whether individual episignature probes are contained within larger DMRs between cases and controls. DMRs could potentially provide a link to downstream gene expression. We first investigated DMRs in an unbiased genome-wide manner by calling DMRs from the 850K DNA methylation array data (n=16 CHD2, n=18 controls) using bumphunter and DMRcate. We predicted 1,684 DMRs from bumphunter and 963 DMRs from DMRcate. These DMRs were intersected, requiring an overlap in the same direction (hyper/hypo) of at least 50bp, to derive a high-confidence DMR list of 712 overlapping regions (349 hyper, 363 hypo). Representative images of these DMRs are shown in Figure S25. These DMRs directly coincide with 86/200 (43%) CHD2 450K episignature probes and an increased 90/200 (45%) CHD2 850K episignature probes (Figure S26, Table S8). Thus, the CHD2 episignature is characterized by DMRs, and this overlap increases by four probes for the CHD2 850K episignature.

Increased CpG Resolution and Genomic Coverage of Differentially Methylated Regions Using Whole Genome-Bisulfite Sequencing

Due to limited genomic coverage, DNA methylation arrays can be skewed in their representation of CpGs across the genome, as evidenced by their tendency to bias gene set analyses[72]. To better understand the DMR landscape of *CHD2* and investigate DMRs at higher CpG resolution,

we performed WGBS with coverage of >20,000,000 CpGs on three CHD2 trios and one singleton. We derived 11,019 DMRs from DSS, 4,078 DMRs from DMRcate, and 3,665 DMRs that overlap between both callers (2420 hyper, 1235 hypo). To determine the robustness of this approach, we manually inspected DMRs with a methylation difference of at least 20% (n=207 DMRs, 146 hyper, 61 hypo) by examining the reads in all 3 trios in IGV and confirmed 169/207 DMRs, yielding a true call rate of 81.6%. Representative DMRs called from WGBS are shown in Figure S27. We then investigated the overlap of episignature probes with the WGBS DMRs with a methylation difference of at least 5% and found direct overlap with 76/200 (38%) CHD2 450K episignature probes and an increased 94/200 (47%) CHD2 850K episignature probes (Figure 4D, Figure S26). Thus, considering the increased genomic coverage afforded by WGBS and increased DMRs, it is unsurprising that a higher proportion of CHD2 850K episignature probes overlap with DMRs (Figure S26, Table S8). Notably, for nearly all probes found within DMRs, those DMRs could be better visualized from the WGBS data due to the lack of probe coverage on the array. Thus, we have confirmed using an orthogonal approach with higher CpG coverage that the CHD2 episignature is characterized by DMRs.

We further investigated DMR calls by functionally annotating them using the annotatr. We first examined the representation of CpG islands, CpG shores, CpG shelves, and interCpG Island (interCGI) regions for DMRs (Figure S28). We find that most DMRs called exclusively from WGBS are located at interCGI regions compared to DMRs called from the array or overlap of both, likely due to the bias of gene-enriched regions on the array compared with increased genomic coverage of WGBS. We also annotated DMRs with gene annotations (Figure S29) and found similar patterns across DMRs called by the 850K array, WGBS, or both, especially for DMRs called with a methylation difference of at least 5% between CHD2 and controls. Notably, we show how the global CHD2 episignature is characterized by DMRs (Figure S30) that correspond to gene regulatory regions and therefore, likely affect underlying disease biology.

DISCUSSION

A major challenge in rare disease genetics is determining molecular causes in unsolved cases. Even if ES or comprehensive GS of trios identifies all *de novo* and recessively inherited coding and noncoding variants, prioritizing and functionally interpreting candidate variants is challenging. In the case of the DEEs, this difficulty is further compounded by immense phenotypic and genetic heterogeneity. Genome-wide DNA methylation analysis represents an innovative approach to discovering genetic etiologies by investigating rare DMRs and screening for DNA methylation signatures. Notably, rare DMRs and episignatures can be assessed with cost-effective, high-throughput DNA methylation arrays using blood-derived DNA. Here, we performed genome-wide DNA methylation analysis on 516 individuals with unsolved DEEs and identified causal or candidate etiologies in 10 individuals: five from rare DMR analysis (Table 1) and five from episignature screening (Table 2). Thus, the diagnostic yield of genome-wide methylation analysis in individuals with unsolved DEEs is nearly 2%, similar to the added diagnostic yield of GS after ES or gene panel[73,74]. A study of unsolved ND-CA showed a similar 2-3% increase in diagnostic yield using episignature analysis[52].

We have performed rare outlier DMR analysis of methylation array data for a cohort of individuals with unsolved DEEs and uncovered various underlying DNA variants using ONT long-read sequencing. These include a X;13 translocation, CGG repeat expansions, and copy number variants. We first validated a subset of outlier DMRs using targeted EM-seq enriched for 3.98M CpGs, a highly effective bisulfite-free, enzyme-based conversion method for detecting CpG methylation by sequencing. Targeted EM-seq has several advantages to bisulfite-based array approaches, including minimizing DNA damage, lowering input requirements (picograms of DNA), and detecting more CpGs[34]. We found that all DMRs were confirmed using the EM-seq approach, and the greater number of CpGs detected compared to the methylation array afforded higher

758 resolution to interpret DMRs. Future high-throughput DNA methylation analyses could consider
759 using EM-seq for validation or discovery.

760 We report an individual with 27 outlier hypermethylation events along chr13q detected
761 through the rare DMR analysis. Using ONT whole-genome long-read sequencing, we identified a
762 *de novo* X;13 translocation showing that the hypermethylation identified the likely cause of
763 disease. This discovery was enabled without the need for live cellular material, which is typically
764 required by classical cytogenetics approaches. This child passed away in infancy due to the
765 severity of the disease, and this approach provided a diagnosis postmortem using banked
766 genomic material.

767 We also found that several individuals displayed hypermethylation of loci associated with
768 known or novel CG-rich repeat expansions. These regions include the 5'UTR and intron 1 of the
769 epilepsy candidate gene *CSNK1E*, the 5'UTR of the neurodevelopmental disorder gene *DIP2B*,
770 and the 5'UTR of the uncharacterized gene *BCLAF3*. We report the occurrence of
771 hypermethylation, a CGG repeat expansion, and reduced expression of *CSNK1E* among three
772 unrelated individuals with unsolved DEEs and a mildly affected parent. *CSNK1E* has been
773 implicated in the circadian rhythm[75,76], and variation causes a familial advanced sleep phase
774 syndrome (FASPS)[77]. Variation also produces a rapid eye movement phenotype in a knockout
775 mouse model[78]. Interestingly, all our probands with DEEs and the mildly affected parent with
776 *CSNK1E* hypermethylation and a repeat expansion report sleep-related phenotypes
777 (Supplemental Phenotype data). Our results indicate that there is an enrichment of *CSNK1E*
778 hypermethylation in individuals with DEE compared to controls in our cohort combined with those
779 previously reported[14] (Fisher's Exact P=0.0185), suggesting that further studies to determine if
780 *CSNK1E* variation contributes to DEEs are warranted.

781 One male proband with unsolved DEE displayed *de novo* outlier hypermethylation in a
782 region annotated as intergenic on the GRCh37/hg19 genome build and at the 5'UTR of *BCLAF3*

on the GRCh38/hg38 genome build. Using ONT long-read sequencing, we discovered a novel CGG repeat expansion in exon 1 of *BCLAF3* in this proband inherited from his unaffected parent. The parent's long-read data displayed skewed X-inactivation against the expanded allele, and this was confirmed to be more global using an enzyme-based DNA methylation assay to profile the *AR* and *HUMARA* loci (Table S6)[68]. Skewed X-inactivation may explain why the parent does not have a detectable DNA methylation abnormality at this locus and could provide a mechanism to circumvent any functional consequences of the *BCLAF3* abnormality. While *BCLAF3* has been previously predicted to be a potential disorder-associated gene on chrX[79], little is known about its function or disease associations. Thus, further work is needed to investigate whether this abnormality is present in other individuals and if loss of this gene on chrX in males could cause a DEE.

We performed episignature screening of our unsolved DEE cohort using the EpiSign™ v4 classifier, which contains 90 episignatures representing 70 disorders encompassing 96 genes/genomic regions. We found six individuals with unsolved DEEs harbored positive episignatures concordant with their phenotypes. We reviewed or reanalyzed available or newly generated ES or GS data and identified pathogenic variants in the episignature-associated genes in 5/6 individuals. In the individual with a pathogenic *SETD1B* variant, one parent was unavailable for genetic testing to segregate the sequence variant. Thus, the positive episignature finding provided supportive information for genetic diagnosis in lieu of inheritance data. Episignatures can serve to screen for disorders that have broad, overlapping phenotypes and identify individuals who may not have the classical features of a specific neurodevelopmental syndrome or DEE. For instance, most DEEs have a phenotypic spectrum, so individuals with different etiology, developmental trajectories, or subtle dysmorphic features may escape diagnosis until a molecular etiology is found.

The top 27 most implicated genetic causes of DEEs explain 80% of DEEs[7]. However, only 1/27 genes (*CHD2*) has a clinically validated episignature. Like *CHD2*, 58/59 genes with robust episignatures localize to the nucleus and are associated with DNA binding, transcriptional regulation, and histone interactions. Since DNA methylation occurs in the nucleus, most genes for which episignatures have been derived are directly or indirectly involved in the epigenetic and transcriptional machinery. Whereas the top 27 DEE genes are associated with a range of cellular processes[5], only a minority are associated with direct DNA interactions, and only 10 of the top 27 most frequent DEE genes are annotated to localize to the nucleus at least partially. The only gene with a clinically validated episignature not involved in any nuclear activity is *SLC32A1*, which encodes solute carrier family 32 member 1 (*SLC32A1*, MIM:616440) responsible for inhibitory neurotransmission, and variants in this gene cause a DEE[80]. Unfortunately, *SLC32A1* is not among the most common ~60 DEE genes. Therefore, the diagnostic utility of episignatures for DEEs would increase when we can confidently derive episignatures for more DEE genes, such as ion channel, synaptic transmission, and metabolic genes.

Episignature derivation is further complicated by the existence of variant-specific episignatures that exist for a subgroup of variants within a gene (e.g.*SMARCA2*[50,81]) or a set of common genes within similar pathways (e.g.Coffin-Siris syndrome episignature, due to variants in *ARID1A* (MIM: 603024), *ARID1B* (MIM:614556), *SMARCB1* (MIM:601607), and *SMARCA4* (MIM:603254), and *SOX11* (MIM:600898)[50]. Thus, there is not only a need to derive episignatures for more epilepsy-related genes but also to analyze variants for testing based on variant type (i.e. missense, nonsense) and protein domain, which may segregate with phenotypes. For instance, our cohort included two females with solved DEEs and pathogenic truncating variants in the *SMC1A* gene located on chromosome X. Neither had a positive episignature for *SMC1A* for Cornelia de Lange syndrome (CdLS), which is usually due to missense or in-frame small indels proposed to have a dominant negative effect. Truncating, loss-of-function variants, however, are

found exclusively in girls with DEEs. The difference in underlying disease mechanism likely impacts the composition of the distinct probe sets contained within the episignatures. Discordant or unusual findings like this example underscore additional considerations when deriving and interpreting episignatures. We came across five individuals reported as male whose methylation pattern on the X chromosome suggested two X chromosomes. Of 2/5 of these individuals who had LRS, a genotype of XXY was confirmed, which is consistent with a diagnosis of Klinefelter syndrome. More unexpected and incidental findings will arise as a greater number of episignatures are derived, and methylation testing becomes more routine.

Episignatures for many epilepsy-related genes are currently in development. As more episignatures are clinically validated, re-analysis of previously generated methylation array data from unsolved individuals will identify pathogenic findings, akin to re-analysis of exome sequencing data for new epilepsy genes years after initial sequencing was performed[82]. We found that episignature analysis was useful for clarifying VUSs, including an individual annotated as solved for *CHD2* displaying a VUS, which was re-assessed as benign based on a negative CHD2 episignature result. We anticipate that episignatures will also be useful for interpreting the impact of noncoding variants.

There are additional considerations when determining the utility of DNA methylation analysis for the molecular diagnosis of individuals with DEEs. Firstly, the diagnostic utility will vary depending on when the individual receives the test relative to other genetic testing modalities. In our study, we analyzed DNA from individuals with DEEs who had remained unsolved after undergoing extensive genetic testing, including gene panels, microarrays, exome, and genome sequencing. As DNA methylation testing becomes increasingly accessible to newly diagnosed individuals with DEEs and as the number of epilepsy-relevant genes with robust episignatures grows, the utility of DNA methylation analysis in unsolved DEEs may increase and guide which regions should be sequenced to identify causal variants.

857 DNA methylation information can be readily assessed from both ONT long-read
858 sequencing and PacBio long-read sequencing data. Therefore, when long-read sequencing
859 becomes more available, there is potential for an “all-in-one” approach to genetic testing whereby
860 individuals can simultaneously be assessed for sequence variants, structural abnormalities, and
861 rare DNA methylation changes. While it is advantageous to study rare DMRs and their potential
862 underlying DNA defects using the same technology, applying episignatures to long-read
863 sequencing data is uncertain and may require new computational approaches to re-derive and
864 validate episignatures on each platform. As long-read sequencing produces far more data than
865 arrays (>20,000,000 CpGs versus ~850,000 CpGs), this will offer an opportunity to interrogate
866 DNA methylation more broadly and deeply.

867 As advances in sequencing technologies allow DNA methylation datasets to get larger,
868 there will be a need to analyze comparative data from controls to generate population-level
869 reference information. For our DMR analysis, we leveraged 450K DNA methylation array outlier
870 DMR calls generated from peripheral blood-derived DNA for >23,000 control individuals[14]. Where
871 possible, we used these data to approximate population frequencies for the DMRs we derived.
872 However, this reference information is not available for 850K exclusive DMRs or whole-genome
873 sequencing DMRs. Thus, interpreting DNA methylation data for unsolved DEEs and other
874 unsolved genetic disorders will improve as we understand more of the methylome, including
875 regions that were only recently resolved on the T2T genome build[83], using appropriate reference
876 datasets from diverse populations.

877 While episignatures provide a robust readout of the genetic etiology, they are composed
878 of individual array probes representing singular CpG sites that may not contribute to
879 understanding the underlying disease mechanism. Given that *CHD2* is the most frequent DEE
880 genes with a robust episignature and has a biological role as a chromatin remodeler, we were
881 interested to use the episignature to understand how DNA methylation relates to underlying *CHD2*

882 pathophysiology. First, we re-defined the episignature on exclusively 850K array probes with an
883 increased sample size from n=9 to n=29 individuals with *CHD2* pathogenic variants. Using DNA
884 methylation array and WGBS, we show that the CHD2 episignature is associated with DMRs
885 between cases and controls. In a recent study, investigators derived DMRs for individuals with
886 pathogenic *HNRNPU* (MIM:617391) variants versus controls in methylation array data from
887 peripheral blood-derived DNA and reported 19 DMRs called with DMRcate (Fischer P<0.01,
888 betacutoff=0.05, minCpG=5)[84]. The comparative number of DMRs we derived for *CHD2* versus
889 control methylation array data under the same conditions using DMRcate is 474 DMRs. This
890 increased number of DMRs may represent the inherent function of CHD2 as a chromatin
891 remodeler that interacts directly with the DNA, whereas HNRNPU forms complexes with RNA.
892 Furthermore, a subset of CHD2 episignature probes overlap with DMRs in the TSS/5'UTR of
893 developmentally relevant genes and might regulate expression (Table S7). For instance, a cluster
894 of hypermethylated episignature probes for the CHD2 450K and 850K episignatures are
895 contained within a larger hypermethylated DMR in the TSS and 5'UTR of *HOXA4* (Figure S31).
896 However, *HOXA4* is not expressed in the blood, and, therefore, would not be expected to be
897 impacted by differential methylation. Thus, we have shown that *CHD2* is associated with DMRs
898 in the blood that correspond with the episignature. Our work suggests that future studies should
899 investigate the CHD2 episignature in disease-relevant tissue types where DMRs are likely to
900 contribute directly to gene dysregulation and disease pathogenesis.

901 Here, we have utilized various DNA methylation analyses to identify causative and
902 candidate etiologies in 2% of our cohort of 516 individuals with unsolved DEEs. While DNA
903 methylation does not explain the majority of DEEs, methylation array yield is comparable to the
904 current added utility of GS[4,73] and remains a low-cost approach that can detect missed genetic
905 etiologies and propose new molecular candidates. Importantly, this yield is expected to increase
906 over time as we interrogate the functional consequences of rare DMRs and better understand

907 which genes and pathways exhibit episignatures, including unraveling inconclusive episignature
908 results. We have also investigated the episignature for the DEE gene *CHD2* in-depth and have
909 provided evidence that the CHD2 episignature is associated with DMRs. DMRs may affect gene
910 expression, especially in disease-relevant tissue types. Furthermore, CHD2 episignatures and
911 associated DMRs may have potential as a biomarker readout for therapeutic testing, as the DNA
912 methylation might potentially be reversed with targeted treatment. Thus, our work highlights the
913 impact of investigating DNA methylation in DEEs, both for the genetic diagnosis of unsolved cases
914 and to augment our understanding of underlying disease function toward the future development
915 of targeted therapies.

916

Declaration of Interests

B.S. is a shareholder in EpiSign Inc, a company involved in commercialization of EpiSign™ software. D.E.M is on a scientific advisory board at ONT and has received travel support from ONT to speak on their behalf. D.E.M is engaged in a research agreement with ONT. D.E.M holds stock options in MyOme. I.E.S. has served on scientific advisory boards for BioMarin, Chiesi, Eisai, Encoded Therapeutics, GlaxoSmithKline, Knopp Biosciences, Nutricia, Rogcon, Takeda Pharmaceuticals, UCB, Xenon Pharmaceuticals, Cerecin; has received speaker honoraria from GlaxoSmithKline, UCB, BioMarin, Biocodex, Chiesi, Liva Nova, Nutricia, Zuellig Pharma, Stoke Therapeutics and Eisai; has received funding for travel from UCB, Biocodex, GlaxoSmithKline, Biomarin, Encoded Therapeutics Stoke Therapeutics and Eisai; has served as an investigator for Anavex Life Sciences, Cerevel Therapeutics, Eisai, Encoded Therapeutics, EpiMinder Inc, Epygenyx, ES-Therapeutics, GW Pharma, Marinus, Neurocrine BioSciences, Ovid Therapeutics, Takeda Pharmaceuticals, UCB, Ultragenyx, Xenon Pharmaceuticals, Zogenix and Zynerba; has consulted for Care Beyond Diagnosis, Epilepsy Consortium, Atheneum Partners, Ovid Therapeutics, UCB, Zynerba Pharmaceuticals, BioMarin, Encoded Therapeutics and Biohaven Pharmaceuticals; and is a Non-Executive Director of Bellberry Ltd and a Director of the Australian Academy of Health and Medical Sciences and the Australian Council of Learned Academies Limited. I.E.S. may accrue future revenue on pending patent WO61/010176 (filed: 2008): Therapeutic Compound; has a patent for *SCN1A* testing held by Bionomics Inc and licensed to various diagnostic companies; has a patent molecular diagnostic/theragnostic target for benign familial infantile epilepsy (BFIE) [PRRT2] 2011904493 & 2012900190 and PCT/AU2012/001321 (TECH ID:2012-009). L.G.S. receives funding from the Health Research Council of New Zealand and Cure Kids New Zealand, is a consultant for the Epilepsy Consortium, and has received travel grants from Seqirus and Nutricia. L.G.S. has received research grants and consultancy fees from Zynerba Pharmaceuticals and has served on and Takeda and Eisai Pharmaceuticals scientific

advisory panels. The Department of Molecular and Human Genetics at Baylor College of Medicine receives revenue from clinical genetic testing conducted at Baylor Genetics Laboratories.

Acknowledgments

We thank all the individuals and their families for participating in this research. Major funding for this project was provided by a grant (#631106) from Citizens United for Research in Epilepsy (CURE). A subset of DNA methylation arrays was provided by the University of Washington Center for Rare Disease Research (UW-CRDR), formerly known as the Center for Mendelian Genomics (CMG), with support from NHGRI grants U01 HG011744, UM1 HG006493 and U24 HG011746 and with enthusiastic support from the late Debbie Nickerson. We gratefully acknowledge support from the Australian Epilepsy Research Foundation grant, Australian National Health and Medical Research Council (NHMRC) Centre for Research Excellence Grant (GNT2006841), NHMRC Synergy Grant (GNT2010562), the Health Research Council of New Zealand, Cure Kids New Zealand, and the Estate of Ernest Hyam Davis and the Tedd and Mollie Carr Endowment Trust. We acknowledge the Epi25 Consortium, which provided exome sequence data for review for a subset of individuals. C.W.L. has been funded through the American Epilepsy Society (AES) predoctoral fellowship and the St. Jude Graduate School of Biomedical Sciences. We would also like to acknowledge the inaugural St. Jude Biohackathon 2022 for coordinating the event that led to a team comprised of C.W.L., P.K., M.D., and W.R., who assembled the MethylMiner pipeline described here. D.E.M. is supported by NIH grant DP5OD033357. Research reported in this manuscript by M.W.H., S.K., H.D., K.C.W., J.A.R., and H.T.C., was supported by the NIH Common Fund, through the Office of Strategic Coordination/Office of the NIH Director under Award Numbers U01HG007709 and U01HG007942. K.L.P. has been funded through the *GRIN2B* foundation and CURE. I.E.S. is also supported by a NHMRC Senior Investigator

Fellowship (GNT1172897). We acknowledge Pratibha Kottapalli and Sanchit Trivedi from the St. Jude Hartwell Center who performed Illumina sequencing for this project. The content is solely the responsibility of the authors and does not necessarily represent the official views of the NIH.

Data and Code Availability

Methylation array data for individuals with unsolved DEEs and those with pathogenic variants in *CHD2* who have given consent for data sharing will be made available through dbGaP. Additional data requests can be directed to H.C.M. The methylation array analysis pipeline used in part of this study for epivariant detection can be accessed on GitHub: https://github.com/stjude-biohackathon/MethylMiner. EpiSign™ is proprietary commercial software and is not publicly available.

Supplemental Information

Supplemental phenotype data, methods, and figures are in the supplemental documents section.

REFERENCES

1 Scheffer, I. E. *et al.* ILAE classification of the epilepsies: Position paper of the ILAE Commission for Classification and Terminology. *Epilepsia* **58**, 512-521 (2017). https://doi.org/10.1111/epi.13709

2 Oliver, K. L. *et al.* Genes4Epilepsy: An epilepsy gene resource. *Epilepsia* **64**, 1368-1375 (2023). https://doi.org/10.1111/epi.17547

3 Poke, G., Stanley, J., Scheffer, I. E. & Sadleir, L. G. Epidemiology of Developmental and Epileptic Encephalopathy and of Intellectual Disability and Epilepsy in Children. *Neurology* **100**, e1363-e1375 (2023). https://doi.org/10.1212/WNL.0000000000206758

4 Palmer, E. E. *et al.* Integrating exome sequencing into a diagnostic pathway for epileptic encephalopathy: Evidence of clinical utility and cost effectiveness. *Mol Genet Genomic Med* **6**, 186-199 (2018). https://doi.org/10.1002/mgg3.355

5 McTague, A., Howell, K. B., Cross, J. H., Kurian, M. A. & Scheffer, I. E. The genetic landscape of the epileptic encephalopathies of infancy and childhood. *The Lancet Neurology* **15**, 304-316 (2016). https://doi.org/10.1016/s1474-4422(15)00250-1

6 Sanchez Fernandez, I., Loddenkemper, T., Gainza-Lein, M., Sheidley, B. R. & Poduri, A. Diagnostic yield of genetic tests in epilepsy: A meta-analysis and cost-effectiveness study. *Neurology* (2019). https://doi.org/10.1212/WNL.0000000000006850

7 Symonds, J. D. & McTague, A. Epilepsy and developmental disorders: Next generation sequencing in the clinic. *Eur J Paediatr Neurol* **24**, 15-23 (2020). https://doi.org/10.1016/j.ejpn.2019.12.008

8 Mefford, H. C. *et al.* Rare copy number variants are an important cause of epileptic encephalopathies. *Ann Neurol* **70**, 974-985 (2011). https://doi.org/10.1002/ana.22645

9 A roadmap for precision medicine in the epilepsies. *The Lancet Neurology* **14**, 1219-1228 (2015). https://doi.org/10.1016/s1474-4422(15)00199-4

10 Bayat, A., Bayat, M., Rubboli, G. & Moller, R. S. Epilepsy Syndromes in the First Year of Life and Usefulness of Genetic Testing for Precision Therapy. *Genes (Basel)* **12** (2021). https://doi.org/10.3390/genes12071051

11 D'Gama, A. M. *et al.* Evaluation of the feasibility, diagnostic yield, and clinical utility of rapid genome sequencing in infantile epilepsy (Gene-STEPS): an international, multicentre, pilot cohort study. *Lancet Neurol* **22**, 812-825 (2023). https://doi.org/10.1016/S1474-4422(23)00246-6

12 Sheidley, B. R. *et al.* Genetic testing for the epilepsies: A systematic review. *Epilepsia* (2021). https://doi.org/10.1111/epi.17141

13 Moore, L. D., Le, T. & Fan, G. DNA methylation and its basic function. *Neuropsychopharmacology* **38**, 23-38 (2013). https://doi.org/10.1038/npp.2012.112

14 Garg, P. *et al.* A Survey of Rare Epigenetic Variation in 23,116 Human Genomes Identifies Disease-Relevant Epivariations and CGG Expansions. *Am J Hum Genet* **107**, 654-669 (2020). https://doi.org/10.1016/j.ajhg.2020.08.019

15 LaCroix, A. J. *et al.* GGC Repeat Expansion and Exon 1 Methylation of XYLT1 Is a Common Pathogenic Variant in Baratela-Scott Syndrome. *Am J Hum Genet* **104**, 35-44 (2019). https://doi.org/10.1016/j.ajhg.2018.11.005

16 Barbosa, M. *et al.* Identification of rare de novo epigenetic variations in congenital disorders. *Nat Commun* **9**, 2064 (2018). https://doi.org/10.1038/s41467-018-04540-x

17 Levy, M. A. *et al.* Novel diagnostic DNA methylation episignatures expand and refine the epigenetic landscapes of Mendelian disorders. *Human Genetics and Genomics Advances* (2021). https://doi.org/10.1016/j.xhgg.2021.100075

18 Aref-Eshghi, E. *et al.* Evaluation of DNA Methylation Episignatures for Diagnosis and Phenotype Correlations in 42 Mendelian Neurodevelopmental Disorders. *Am J Hum Genet* **106**, 356-370 (2020). https://doi.org/10.1016/j.ajhg.2020.01.019

19 Sadikovic, B. *et al.* Clinical epigenomics: genome-wide DNA methylation analysis for the diagnosis of Mendelian disorders. *Genet Med* **23**, 1065-1074 (2021). https://doi.org/10.1038/s41436-020-01096-4

20 Levy, M. A. *et al.* Functional correlation of genome-wide DNA methylation profiles in genetic neurodevelopmental disorders. *Hum Mutat* **43**, 1609-1628 (2022). https://doi.org/10.1002/humu.24446

21 Carvill, G. L. *et al.* Targeted resequencing in epileptic encephalopathies identifies de novo mutations in CHD2 and SYNGAP1. *Nat Genet* **45**, 825-830 (2013). https://doi.org/10.1038/ng.2646

22 Scheffer, I. E. *et al.* Exome sequencing for patients with developmental and epileptic encephalopathies in clinical practice. *Dev Med Child Neurol* **65**, 50-57 (2023). https://doi.org/10.1111/dmcn.15308

23 Parkinson Progression Marker, I. The Parkinson Progression Marker Initiative (PPMI). *Prog Neurobiol* **95**, 629-635 (2011). https://doi.org/10.1016/j.pneurobio.2011.09.005

24 Pidsley, R. *et al.* Critical evaluation of the Illumina MethylationEPIC BeadChip microarray for whole-genome DNA methylation profiling. *Genome Biol* **17**, 208 (2016). https://doi.org/10.1186/s13059-016-1066-1

25 Aryee, M. J. *et al.* Minfi: a flexible and comprehensive Bioconductor package for the analysis of Infinium DNA methylation microarrays. *Bioinformatics* **30**, 1363-1369 (2014). https://doi.org/10.1093/bioinformatics/btu049

26 Leek, J. T., Johnson, W. E., Parker, H. S., Jaffe, A. E. & Storey, J. D. The sva package for removing batch effects and other unwanted variation in high-throughput experiments. *Bioinformatics* **28**, 882-883 (2012). https://doi.org/10.1093/bioinformatics/bts034

27 Johnson, W. E., Li, C. & Rabinovic, A. Adjusting batch effects in microarray expression data using empirical Bayes methods. *Biostatistics* **8**, 118-127 (2007). https://doi.org/10.1093/biostatistics/kxj037

28 Jaffe, A. E. & Irizarry, R. A. Accounting for cellular heterogeneity is critical in epigenome-wide association studies. *Genome Biology* **15**, R31 (2014). https://doi.org/10.1186/gb-2014-15-2-r31

29 Heinz, S. *et al.* Simple combinations of lineage-determining transcription factors prime cis-regulatory elements required for macrophage and B cell identities. *Mol Cell* **38**, 576-589 (2010). https://doi.org/10.1016/j.molcel.2010.05.004

30 Court, F. *et al.* Genome-wide parent-of-origin DNA methylation analysis reveals the intricacies of human imprinting and suggests a germline methylation-independent mechanism of establishment. *Genome Res* **24**, 554-569 (2014). https://doi.org/10.1101/gr.164913.113

31 Zhou, W., Laird, P. W. & Shen, H. Comprehensive characterization, annotation and innovative use of Infinium DNA methylation BeadChip probes. *Nucleic Acids Res* **45**, e22 (2017). https://doi.org/10.1093/nar/gkw967

32 Hamosh, A., Scott, A. F., Amberger, J. S., Bocchini, C. A. & McKusick, V. A. Online Mendelian Inheritance in Man (OMIM), a knowledgebase of human genes and genetic disorders. *Nucleic Acids Res* **33**, D514-517 (2005). https://doi.org/10.1093/nar/gki033

33 Robinson, J. T. *et al.* Integrative genomics viewer. *Nature Biotechnology* **29**, 24-26 (2011). https://doi.org/10.1038/nbt.1754

34 Vaisvila, R. *et al.* Enzymatic methyl sequencing detects DNA methylation at single-base resolution from picograms of DNA. *Genome Res* **31**, 1280-1289 (2021). https://doi.org/10.1101/gr.266551.120

35 Miller, D. E. *et al.* Targeted long-read sequencing identifies missing disease-causing variation. *Am J Hum Genet* **108**, 1436-1449 (2021). https://doi.org/10.1016/j.ajhg.2021.06.006

36 Li, H. Minimap2: pairwise alignment for nucleotide sequences. *Bioinformatics* **34**, 3094-3100 (2018). https://doi.org/10.1093/bioinformatics/bty191

37 Zheng, Z. *et al.* Symphonizing pileup and full-alignment for deep learning-based long-read variant calling. *Nature Computational Science* **2**, 797-803 (2022). https://doi.org/10.1038/s43588-022-00387-x

38 Sedlazeck, F. J. *et al.* Accurate detection of complex structural variations using single-molecule sequencing. *Nat Methods* **15**, 461-468 (2018). https://doi.org/10.1038/s41592-018-0001-7

39 Heller, D. & Vingron, M. SVIM: structural variant identification using mapped long reads. *Bioinformatics* **35**, 2907-2915 (2019). https://doi.org/10.1093/bioinformatics/btz041

40 Jiang, T. *et al.* Long-read-based human genomic structural variation detection with cuteSV. *Genome Biol* **21**, 189 (2020). https://doi.org/10.1186/s13059-020-02107-y

41 Lin, J. H., Chen, L. C., Yu, S. C. & Huang, Y. T. LongPhase: an ultra-fast chromosome-scale phasing algorithm for small and large variants. *Bioinformatics* **38**, 1816-1822 (2022). https://doi.org/10.1093/bioinformatics/btac058

42 *EpiSign v4 Menu*, https://episign.lhsc.on.ca/img/EpiSign_v4_Menu.pdf).

43 Platt, J. C. Probabilistic outputs for support vector machines and comparisons to regularized likelihood methods. *Advances in Large Margin Classifiers* **10** (2000).

44 Sadikovic, B., Levy, M. A. & Aref-Eshghi, E. Functional annotation of genomic variation: DNA methylation episignatures in neurodevelopmental Mendelian disorders. *Hum Mol Genet* **29**, R27-R32 (2020). https://doi.org/10.1093/hmg/ddaa144

45 FastQC: A Quality Control Tool for High Throughput Sequence Data (2010).

46 Dobin, A. *et al.* STAR: ultrafast universal RNA-seq aligner. *Bioinformatics* **29**, 15-21 (2013). https://doi.org/10.1093/bioinformatics/bts635

47 Patro, R., Duggal, G., Love, M. I., Irizarry, R. A. & Kingsford, C. Salmon provides fast and bias-aware quantification of transcript expression. *Nat Methods* **14**, 417-419 (2017). https://doi.org/10.1038/nmeth.4197

48 Brechtmann, F. *et al.* OUTRIDER: A Statistical Method for Detecting Aberrantly Expressed Genes in RNA Sequencing Data. *Am J Hum Genet* **103**, 907-917 (2018). https://doi.org/10.1016/j.ajhg.2018.10.025

49 Yépez, V. A., Murdock, D. R. & Lee, B. Gene expression counts from fibroblast, strand-specific, BCM UDN. *Zenodo* (2020). https://doi.org/10.5281/zenodo.3963474

50 Aref-Eshghi, E. *et al.* BAFopathies' DNA methylation epi-signatures demonstrate diagnostic utility and functional continuum of Coffin-Siris and Nicolaides-Baraitser syndromes. *Nat Commun* **9**, 4885 (2018). https://doi.org/10.1038/s41467-018-07193-y

51 Aref-Eshghi, E. *et al.* Genomic DNA Methylation Signatures Enable Concurrent Diagnosis and Clinical Genetic Variant Classification in Neurodevelopmental Syndromes. *Am J Hum Genet* **102**, 156-174 (2018). https://doi.org/10.1016/j.ajhg.2017.12.008

52 Aref-Eshghi, E. *et al.* Diagnostic Utility of Genome-wide DNA Methylation Testing in Genetically Unsolved Individuals with Suspected Hereditary Conditions. *Am J Hum Genet* **104**, 685-700 (2019). https://doi.org/10.1016/j.ajhg.2019.03.008

53 Ho, D. E., Imai, K., King, G. & Stuart, E. A. Matching as Nonparametric Preprocessing for Reducing Model Dependence in Parametric Causal Inference. *Political Analysis* **15**, 199-236 (2017). https://doi.org/10.1093/pan/mpl013

54 Ritchie, M. E. *et al.* limma powers differential expression analyses for RNA-sequencing and microarray studies. *Nucleic Acids Res* **43**, e47 (2015). https://doi.org/10.1093/nar/gkv007

55 Houseman, E. A. *et al.* DNA methylation arrays as surrogate measures of cell mixture distribution. *BMC Bioinformatics* **13**, 86 (2012). https://doi.org/10.1186/1471-2105-13-86

56 Gu, Z., Gu, L., Eils, R., Schlesner, M. & Brors, B. circlize Implements and enhances circular visualization in R. *Bioinformatics* **30**, 2811-2812 (2014). https://doi.org/10.1093/bioinformatics/btu393

57 Cavalcante, R. G. & Sartor, M. A. annotatr: genomic regions in context. *Bioinformatics* **33**, 2381-2383 (2017). https://doi.org/10.1093/bioinformatics/btx183

58 TreeAndLeaf: Displaying binary trees with focus on dendrogram leaves (R package version 1.12.0., 2023).

59 Fortin, J.-P. *et al.* Functional normalization of 450k methylation array data improves replication in large cancer studies. *Genome Biology* **15**, 503 (2014). https://doi.org/10.1186/s13059-014-0503-2

60 Jaffe, A. E. *et al.* Bump hunting to identify differentially methylated regions in epigenetic epidemiology studies. *Int J Epidemiol* **41**, 200-209 (2012). https://doi.org/10.1093/ije/dyr238

61 Peters, T. J. *et al.* De novo identification of differentially methylated regions in the human genome. *Epigenetics & Chromatin* **8**, 6 (2015). https://doi.org/10.1186/1756-8935-8-6

62 Peters, T. J. *et al.* Calling differentially methylated regions from whole genome bisulphite sequencing with DMRcate. *Nucleic Acids Res* **49**, e109 (2021). https://doi.org/10.1093/nar/gkab637

63 Wu, H. *et al.* Detection of differentially methylated regions from whole-genome bisulfite sequencing data without replicates. *Nucleic Acids Res* **43**, e141 (2015). https://doi.org/10.1093/nar/gkv715

64 Tsutsumi, M. *et al.* A female patient with retinoblastoma and severe intellectual disability carrying an X;13 balanced translocation without rearrangement in the RB1 gene: a case report. *BMC Med Genomics* **12**, 182 (2019). https://doi.org/10.1186/s12920-019-0640-2

65 Chen, X. *et al.* A de novo pathogenic CSNK1E mutation identified by exome sequencing in family trios with epileptic encephalopathy. *Hum Mutat* **40**, 281-287 (2019). https://doi.org/10.1002/humu.23690

66 Sobreira, N., Schiettecatte, F., Valle, D. & Hamosh, A. GeneMatcher: a matching tool for connecting investigators with an interest in the same gene. *Hum Mutat* **36**, 928-930 (2015). https://doi.org/10.1002/humu.22844

67 Winnepenninckx, B. *et al.* CGG-repeat expansion in the DIP2B gene is associated with the fragile site FRA12A on chromosome 12q13.1. *Am J Hum Genet* **80**, 221-231 (2007). https://doi.org/10.1086/510800

68 Kiedrowski, L. A. *et al.* DNA methylation assay for X-chromosome inactivation in female human iPS cells. *Stem Cell Rev Rep* **7**, 969-975 (2011). https://doi.org/10.1007/s12015-011-9238-6

69 conumee: Enhanced copy-number variation analysis using Illumina DNA methylation arrays.

70 Harada, A. *et al.* Chd2 interacts with H3.3 to determine myogenic cell fate. *EMBO J* **31**, 2994-3007 (2012). https://doi.org/10.1038/emboj.2012.136

71 Lamar, K. J. & Carvill, G. L. Chromatin Remodeling Proteins in Epilepsy: Lessons From CHD2-Associated Epilepsy. *Front Mol Neurosci* **11**, 208 (2018). https://doi.org/10.3389/fnmol.2018.00208

72 Geeleher, P. *et al.* Gene-set analysis is severely biased when applied to genome-wide methylation data. *Bioinformatics* **29**, 1851-1857 (2013). https://doi.org/10.1093/bioinformatics/btt311

73 Alfares, A. *et al.* Whole-genome sequencing offers additional but limited clinical utility compared with reanalysis of whole-exome sequencing. *Genet Med* **20**, 1328-1333 (2018). https://doi.org/10.1038/gim.2018.41

74 Palmer, E. E. *et al.* Diagnostic Yield of Whole Genome Sequencing After Nondiagnostic Exome Sequencing or Gene Panel in Developmental and Epileptic Encephalopathies. *Neurology* **96**, e1770-e1782 (2021). https://doi.org/10.1212/WNL.0000000000011655

75 Vielhaber, E., Eide, E., Rivers, A., Gao, Z. H. & Virshup, D. M. Nuclear entry of the circadian regulator mPER1 is controlled by mammalian casein kinase I epsilon. *Mol Cell Biol* **20**, 4888-4899 (2000). https://doi.org/10.1128/mcb.20.13.4888-4899.2000

76 Lee, C., Weaver, D. R. & Reppert, S. M. Direct association between mouse PERIOD and CKIepsilon is critical for a functioning circadian clock. *Mol Cell Biol* **24**, 584-594 (2004). https://doi.org/10.1128/mcb.24.2.584-594.2004

77 Toh, K. L. *et al.* An hPer2 phosphorylation site mutation in familial advanced sleep phase syndrome. *Science* **291**, 1040-1043 (2001). https://doi.org/10.1126/science.1057499

78 Zhou, L. *et al.* The circadian clock gene Csnk1e regulates rapid eye movement sleep amount, and nonrapid eye movement sleep architecture in mice. *Sleep* **37**, 785-793, 793A-793C (2014). https://doi.org/10.5665/sleep.3590

79 Leitao, E. *et al.* Systematic analysis and prediction of genes associated with monogenic disorders on human chromosome X. *Nat Commun* **13**, 6570 (2022). https://doi.org/10.1038/s41467-022-34264-y

80 Platzer, K. *et al.* De Novo Missense Variants in SLC32A1 Cause a Developmental and Epileptic Encephalopathy Due to Impaired GABAergic Neurotransmission. *Ann Neurol* **92**, 958-973 (2022). https://doi.org/10.1002/ana.26485

81 Cappuccio, G. *et al.* De novo SMARCA2 variants clustered outside the helicase domain cause a new recognizable syndrome with intellectual disability and blepharophimosis distinct from Nicolaides-Baraitser syndrome. *Genet Med* **22**, 1838-1850 (2020). https://doi.org/10.1038/s41436-020-0898-y

82 Liu, P. *et al.* Reanalysis of Clinical Exome Sequencing Data. *N Engl J Med* **380**, 2478-2480 (2019). https://doi.org/10.1056/NEJMc1812033

83 Nurk, S. *et al.* The complete sequence of a human genome. *Science* **376**, 44-53 (2022). https://doi.org/10.1126/science.abj6987

84 Rooney, K. *et al.* DNA methylation episignature and comparative epigenomic profiling of HNRNPU-related neurodevelopmental disorder. *Genet Med*, 100871 (2023). https://doi.org/10.1016/j.gim.2023.100871

1213

Tables and Table Legends

Table 1. Summary of epivariants and underlying DNA defects identified in this study.

Location	Gene	Direction	Underlying DNA Defect	Inheritance	Probands (n)
chr13	chr13:multiple	Hyper	X;13 translocation (p)	*De novo*	1
Xp22	*BCLAF3*	Hyper	CGG repeat (c)	*De novo*	1
22q13	*CSNK1E*	Hyper	CGG repeat (c)	Inherited	2 + 1 match
12q13	*DIP2B*	Hyper	CGG repeat (c)	Inherited	1
2p16	*CFAP36/CCDC104*	Hyper	Tandem duplication (b)	Inherited	1
2q37.3	chr2:multiple	Hypo	Deletion (b)	Inherited	1
15q24	*LINGO1*	Hypo	Deletion (b)	Inherited	4

List of epivariation findings from screening cohort with unsolved DEEs for rare outlier DNA methylation changes. Molecular findings are considered p=pathogenic, c=candidate, and b=benign.

1214

Table 2. Summary of episignatures and causative sequence variants identified in this study.

Gene	Signature	MVP	Genomic Variant (hg38)	Consequence	Inheritance
ANKRD11	KGBS/ MRD23	0.854	chr16:89284030 G>A	p.Arg838Ter (p)	*De novo*
		0.989	chr16:89279671 C>A	p.Glu2291Ter (p)	*De novo*
SETD1B	IDDSELD	0.763	chr12:121822939 C>T	p.Arg1454Ter (p)	Unknown
TET3	BEFAHRS	0.327	chr2:74102031 dup	p.Thr1749HisfsTer5 (p)	Inherited
UBE2A	MRXSN	0.149	chrX:119583172 G>A	p.Ala126Thr (p)	Inherited
KDM2B	KDM2B	0.982	chr12:121520986 C>G	p.Arg349Pro (u)	Inherited

List of episignature findings from screening unsolved. Methylation Variant Pathogenicity (MVP) scores shown. Molecular findings are considered p=pathogenic or u=variant of uncertain significance.

1215

1216 **Figures and Figure Legends**

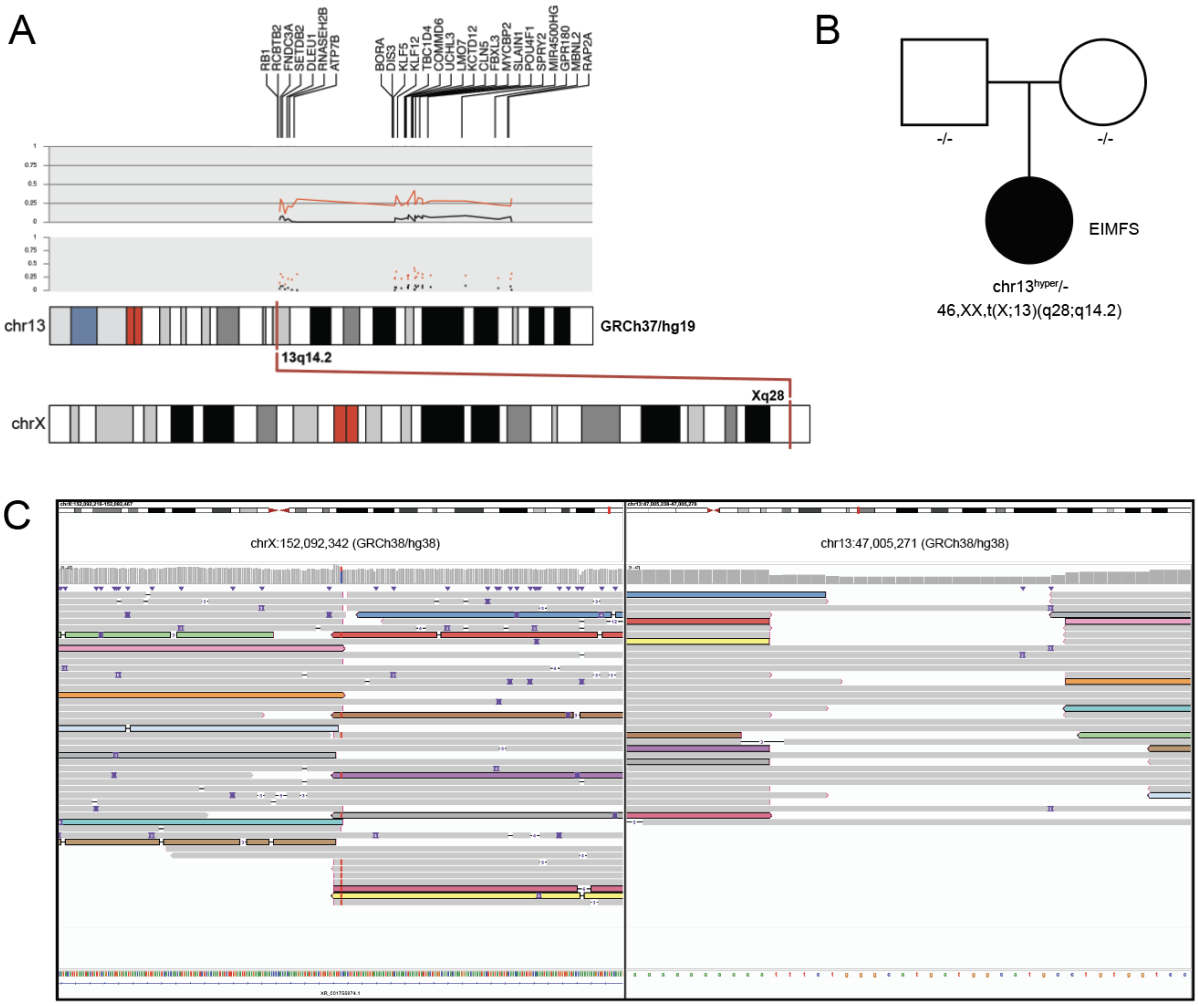

1217

1218 **Figure 1**: Rare outlier DMR analysis identifies chromosomal hypermethylation caused by X;13
1219 translocation. **A.** Graphical representation of chr13 rare hypermethylation events in a proband
1220 with unsolved DEE. The upper portion of the track displays the genes on chr13 for which
1221 hypermethylation events were called. The two grey panels (upper=line, lower=dot) depict β-
1222 values for the average of the proband's array replicates (red) and the average of the parents'
1223 array data (black) for a representative probe within each DMR (n=27). Subtle hypermethylation
1224 hovering around ~25% can be seen for the proband compared to the parents. The lower track
1225 shows chromosomal locations of the DMRs of the X;13 translocation. **B.** Pedigree showing that

chr13 hypermethylation events and the X;13 translocation occured *de novo*. **C.** IGV view of ONT LRS data for chrX (left) and chr13 (right). Some, but not all, reads spanning the translocation are colored to show that they span the breakpoint.

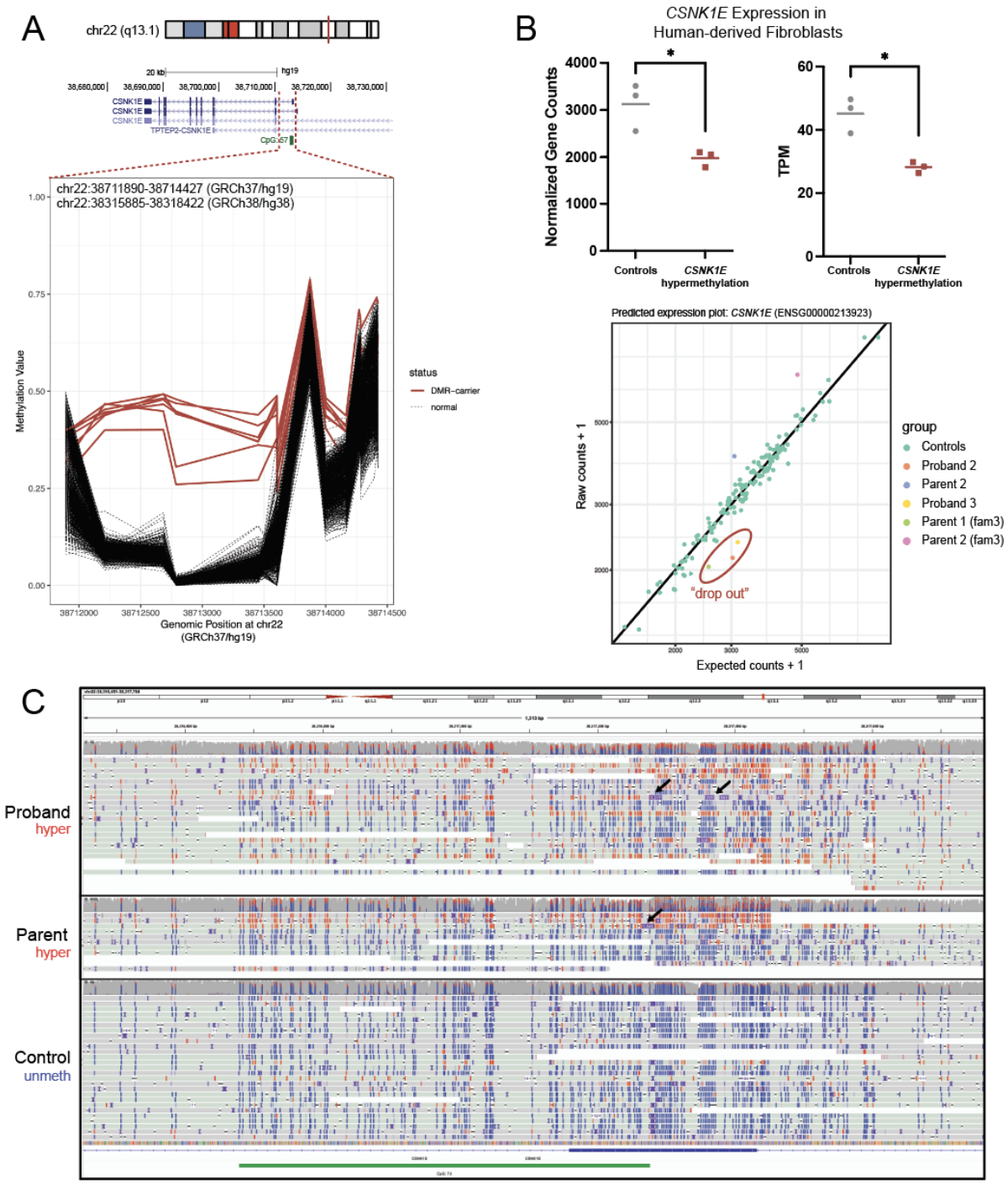

Figure 2: Rare outlier DMR analysis identifies tandem repeat expansions. **A.** DMR plot depicting outlier hypermethylation of the *CSNK1E* 5'UTR and intron 1 in two probands with unsolved DEEs (three replicates across both for a total of five samples), one parent, and one unaffected control

(total n=7 red lines) detected through epivariation analysis. **B.** The upper panel shows expression values from RNA-seq of human-derived fibroblasts for individuals with *CSNK1E* hypermethylation compared to control methylation levels. Significance between groups was determined by a two-tailed paired t-test (p=0.029 for gene counts and p=0.0169 for transcripts per million or TPM). A representative predicted expression plot from drop-out analysis using the OUTRIDER algorithm is shown at the lower portion of the panel. See Figure S9 for the individual OUTRIDER plots for each family and significance information. **C.** Unphased IGV view of LRS data showing CpG sites that are methylated (red) and unmethylated (blue). The CGG repeat expansion seen in the proband was inherited from the parent and is shown as purple squares denoting insertions in the reads (black arrows); not all reads that are methylated show the insertion as they terminated within the inserted sequence and are clipped by the alignment process.

1246

Figure 3: Summary Methylation Variant Pathogenicity (MVP) score for all individuals positive for Episign™ v4 Episignature analysis. A Methylation Variant Pathogenicity (MVP) score (between 0 and 1) was generated to represent the confidence of prediction for the specific episignature on the EpiSign™ v4 clinical classifier that the SVM was trained to detect. Each colored circle represents a different individual and its associated MVP score for each of the episignatures on the EpiSign™ v4 clinical classifier. Final classification for a specific EpiSign™ disorder includes a combination of MVP score, hierarchical clustering, and multidimensional scaling (MDS) review.

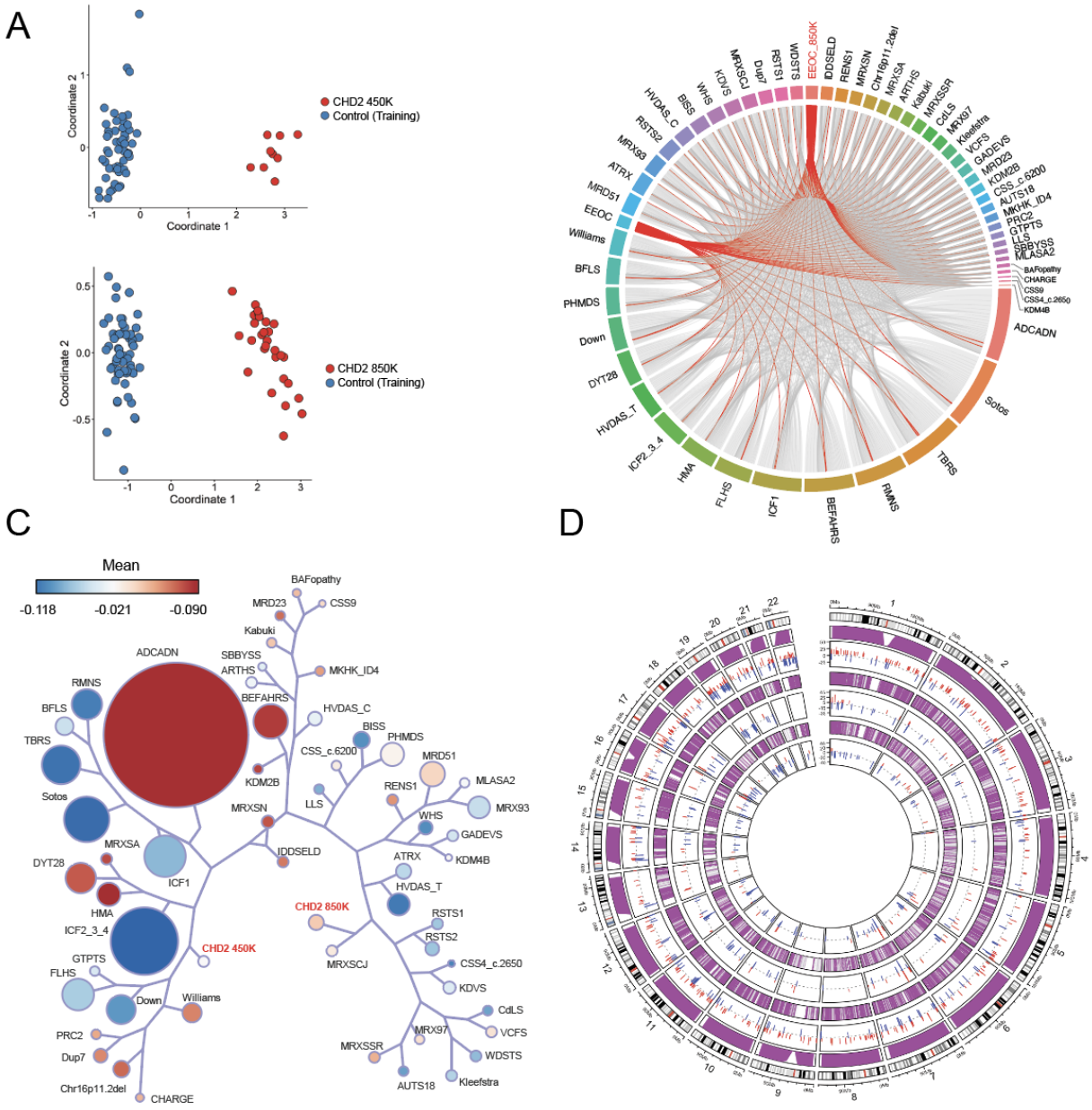

1247

1248 **Figure 4**: Insights from the *CHD2* Episignature. **A**. Multidimensional scaling (MDS) plot showing
1249 clustering of individuals with pathogenic *CHD2* variants (red, upper) for the previously described
1250 *CHD2* 450K (n=9) episignature with shared 450K and 850K array probes clusters away from the
1251 controls (blue) The refined *CHD2* 850K (n=29) episignature (red, lower) clusters away from
1252 unaffected controls (blue). **B**. Circos plot representing shared probes between episignatures.
1253 Differentially methylated probes (DMPs) shared between the CHD2 850K cohort (bold red), CHD2

450K cohort (red), and 55 other episignatures on EpiSign with functional correlation analysis previously published[20]. The thickness of the connecting lines corresponds to the number of probes shared between the cohorts. **C**. Tree and leaf visualization of Euclidean clustering of episignatures. Tree and leaf visualization for all 57 cohorts using the top 500 DMPs for each group (for cohorts with less than 500 DMPs, all DMPS were used). Cohort samples were aggregated using the median value of each probe within a group. A leaf node represents a cohort, with node sizes illustrating relative scales of the number of selected DMPs for the respective cohort, and node colors are indicative of the global mean methylation difference, a gradient of hypomethylation (blue) or hypermethylation (red). **D**. Circular karyotype plot showing overlap of *CHD2* 450K episignature probes (inner circle, n=200), with *CHD2* 850K episignature probes (middle circle, n=200), and WGBS DMRs derived with at least a 15% methylation difference for the condensed visual representation (outer circle, n=411). Each line depicts a probe or DMR where red denotes hypermethylation and blue denotes hypomethylation. The purple tracks depict coverage of the 450K array probes (inner), 850K EPIC array probes (middle), and WGBS reads (outer). Refer to Figure S29 for linear karyotype DMR plots for chr1-22.